Ore Geology Reviews 135 (2021) 104218

Contents lists available at ScienceDirect

Ore Geology Reviews

journal homepage: www.elsevier.com/locate/oregeorev

# Difference in the nature of ore-forming magma between the Mesozoic porphyry Cu-Mo and Mo deposits in NE China: Records from apatite and zircon geochemistry

Pan Qu [a,b,c], Ning-Bo Li [a,c,*], He-Cai Niu [a,c], Qiang Shan [a,c], Qiang Weng [a,b,c], Xiao-Chen Zhao [a,b,c]

[a] CAS Key Laboratory of Mineralogy and Metallogeny/Guangdong Provincial Key Laboratory of Mineral Physics and Materials, Guangzhou Institute of Geochemistry, Chinese Academy of Sciences, Guangzhou 510640, China
[b] University of Chinese Academy of Sciences, Beijing 100049, China
[c] CAS Center for Excellence in Deep Earth Science, Guangzhou, 510640, China

ARTICLE INFO

*Keywords:*
Apatite and zircon
Halogens
Water contents
Differences between porphyry Cu-Mo and Mo deposits
NE China

ABSTRACT

Porphyry Cu-Mo and Mo deposits are the most important source of Mo in the world, but factors controlling their difference remain enigmatic. In recent years, many Mesozoic porphyry Cu-Mo and Mo deposits have been discovered in NE China, which provides a good opportunity to explore the difference between the Cu-Mo and Mo mineralization. In this region, porphyry Cu-Mo deposits (Wunugetushan, Jinchanggou) are distributed along the subduction zone, while the porphyry Mo deposits (Luming, Fu'anpu, Daheishan) are far away from the subduction zone. On the basis of whole rock geochemical studies, we present a comprehensive investigation on the apatite and zircon from Mesozoic typical porphyry Cu-Mo deposits and Mo deposits, in order to reveal the nature of parent magma constraints on Cu-Mo and Mo mineralization. Whole-rock geochemistry, in-situ apatite Sr-Nd and zircon Hf isotopic compositions from these granites in porphyry Cu-Mo and Mo deposits indicate that these granites originated from a juvenile crustal source. Apatites from the porphyry Cu-Mo mineralized granites show relatively high Cl and low F contents, accompanied by enrichment of fluid-mobile elements Ba and Sr, indicating that the magmatic source of porphyry Cu-Mo deposits were modified by subducted slab-derived fluids. In comparison, apatites from the porphyry Mo mineralized granites have high F and low Cl contents with correspondingly high F/Cl ratios, suggesting that these granites mainly formed in juvenile crustal dehydration self-metasomatism under the intra-continental environment. Additionally, apatites from porphyry Cu-Mo mineralized granites have higher OH contents than those from porphyry Mo mineralized granites, indicating that the original melt of porphyry Cu-Mo system was more hydrous, consistent with their higher (Ce/Nd)/Y and lower Dy/Yb ratios of zircon. It is here proposed that the formation of porphyry Cu-Mo deposits in NE China are related to partial melting of the juvenile crust, which metasomatized by slab-derived Cl-enriched fluids with carry significant amounts of Cu, whereas the porphyry Mo deposits are related to partial melting of juvenile crustal material with released F-enriched fluids by the dehydration of hydrous minerals.

## 1. Introduction

Porphyry deposits are the Earth's most important source of Cu and Mo, accounting for approximately 60% of world Cu production and 95% of world Mo production (Sinclair, 2007; Cooke, 2005; Seedorff et al., 2005; Sillitoe, 2010). In addition, a significant amount of Mo is also produced from porphyry Cu (-Mo) deposits (Sinclair, 2007; Chen et al., 2017b and references therein). Therefore, the Mo/Cu ratios and zonation are of economic importance, and the geologic causes for the difference of Cu-Mo mineralization have drawn significant attention for decades. Xie et al. (2017) proposed that the nature of the magma plays an essential role in the differences between porphyry Cu and Mo deposits. Zajacz et al. (2008) proposed that the presence of HCl in the fluid phase control the Cu and Mo partitioning from aspects of experiments.

* Corresponding author at: CAS Key Laboratory of Mineralogy and Metallogeny/Guangdong Provincial Key Laboratory of Mineral Physics and Materials, Guangzhou Institute of Geochemistry, Chinese Academy of Sciences, Guangzhou 510640, China.
*E-mail address:* liningbo@gig.ac.cn (N.-B. Li).

https://doi.org/10.1016/j.oregeorev.2021.104218
Received 22 January 2021; Received in revised form 13 April 2021; Accepted 4 May 2021
Available online 12 May 2021

Zhou et al. (2018) suggested that prolonged fractional crystallization led to Mo-rich and high magma water content favor the formation of Cu-Mo deposits from the perspective of whole rock geochemistry of the Dongbulage Mo and Taibudai Cu-(Mo) porphyry deposits in NE China. Tang et al. (2019) reported that the Mo (Cu) mineralization system formed from F-rich magmatic-hydrothermal fluids whereas the Cu (Mo) mineralization system formed from Cl-rich magmatic-hydrothermal fluids through investigation of magmatic and hydrothermal biotites in the Bangpu porphyry Mo (Cu) deposit, Tibet. To sum up, the nature of ore-forming magma (including magma source and composition) exerts a significant control on the styles of Cu-Mo and Mo mineralization. Nevertheless, the whole rock geochemistry cannot well constrain the nature of parental magma due to the mineralized alteration and weathering.

Apatite [$Ca_5(PO_4)_3(F, OH, Cl)$] is an ideal choice that can reflect the geochemical characteristics of their host rocks and preserve the information of the parental magma. Apatite is a common accessory mineral in porphyry Cu-Mo and Mo deposits (Bouzari et al., 2016). In general, it

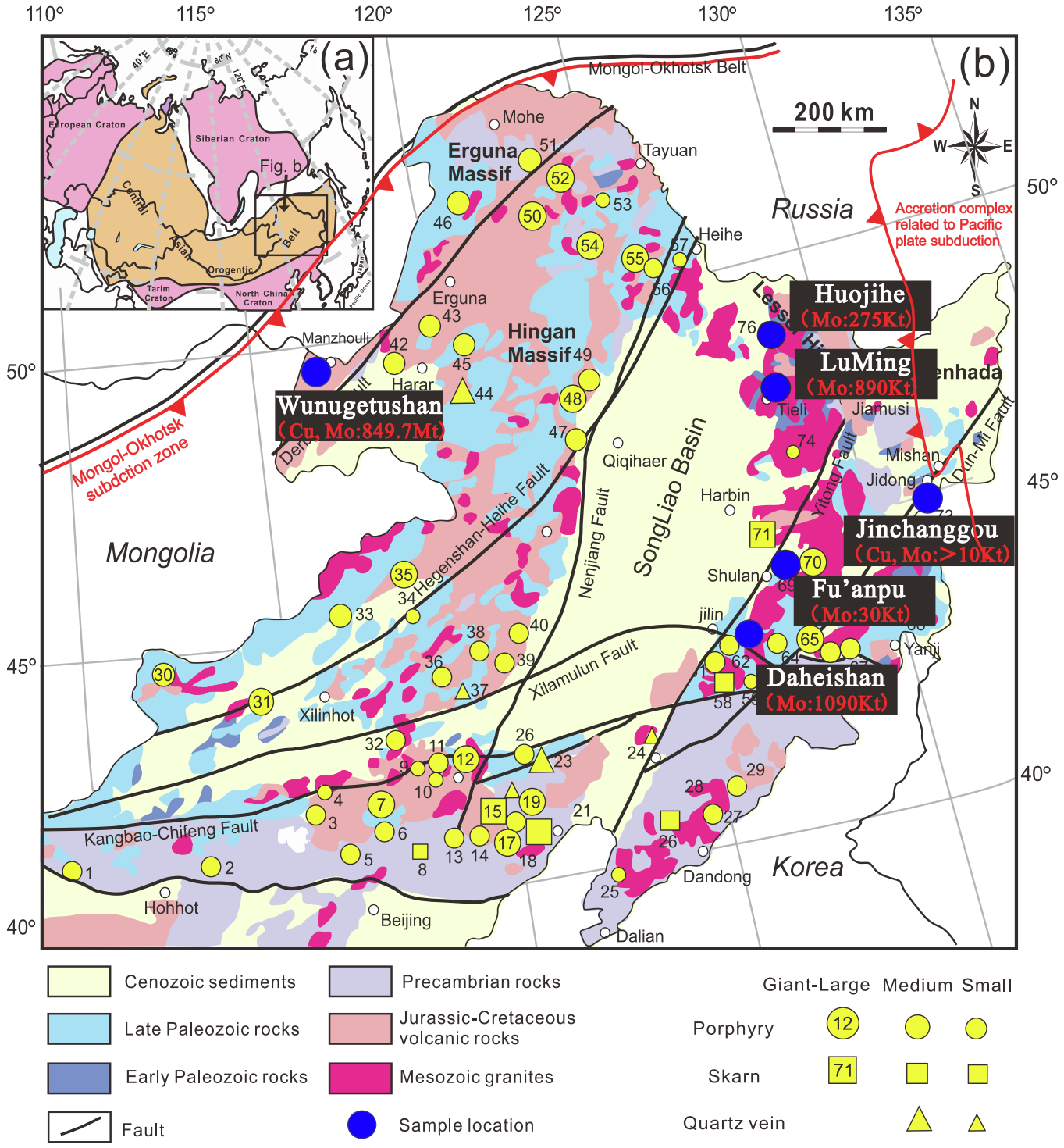


**Fig. 1.** (a) Schematic map showing the location of NE China (modified from Safonova and Santosh, 2014); (b) Geology map of NE China and surrounding regions, showing the distribution of Mesozoic Mo-bearing deposits (modified after Chen et al., 2017b).

can resist weathering and low-grade metamorphism and thus preserve the original chemical compositions of parental magma, especially apatite wrapped in rock-forming minerals (such as K-feldspar and biotite) can effectively avoid the post-hydrothermal alteration (Creaser and Gray, 1992; Mathez and Webster, 2005). Apatite can incorporate a variety of elements, including halogens (F and Cl), Na, S, Fe, Mn, Ba, Sr and REE, which are considerably sensitive to the changes in magmatic composition and evolution, and has been proven useful in revealing details about petrogenetic processes (Chu et al., 2009; Doherty et al., 2014), e.g., magma crystallization history and geologic setting (Miles et al., 2013; Bruand et al., 2014; Webster and Piccoli, 2015). Apatite also has displayed great potential in metallogenic studies (Barth et al., 2013; Bouzari et al., 2016; Mao et al., 2016), such as Cl:F:OH proportions can be used to indicate the ore genesis and evaluate the physiochemical conditions of ore-forming processes (Chu et al., 2009; Douce et al., 2011; Kusebauch et al., 2015). In addition, Sr-Nd isotopes of apatite have been used to constrain the nature of magmatic source (Cao et al., 2019; Palma et al., 2019). Zircon ($ZrSiO_4$) is also a ubiquitous accessory mineral in granite and relatively resistant to weathering (Hoskin and Schaltegger, 2003). Zircon can incorporate a variety of trace elements during crystallization, including rare-earth elements (REE), U, Th, and Ti, and preserve the isotopic composition of its parent magma at the time of crystallization (Zeng et al., 2017). Multiple isotopic systems (e.g., U–Pb, and Hf isotopes) of zircon have been explored to reveal crystallization age and magma sources (Kemp et al., 2007).

Northeastern (NE) China is a significant Mo polymetallic metallogenic province (Fig. 1a; Gao et al., 2017). The latest findings show that porphyry Mo deposits in NE China contain over 11.4 Million tons of Mo, making this the largest Mo metallogenic province in China (Shu et al., 2016). Meanwhile, although lack of porphyry Cu deposits in the polymetallic metallogenic province, some porphyry Cu-Mo deposits are distributed in the region. Almost all of porphyry Cu-Mo deposits are located along the subduction zones, while the porphyry Mo deposits are far away from the subduction zone (Fig. 1b; Chen et al., 2017b). To better understand the factors controlling on Cu-Mo and Mo mineralization styles, five typical porphyry Cu-Mo and Mo deposits located in NE China, namely the Wunugetushan (WS) and Jinchanggou (JC) Cu-Mo deposits, and the Luming (LM), Fu'anpu (FA) and Daheishan (DHS) Mo deposits, have been selected in this study (Fig. 1b). In this paper, we present mineral assemblage observations, whole-rock geochemistry, integrated elemental and isotopic geochemistry of apatite and zircon from these porphyry Cu-Mo and Mo deposits in NE China. The results are used to evaluate the physical and chemical conditions associated with the ore forming magma leading to the formation of the deposit, and to reveal the factors controlling the diversity of Cu-Mo and Mo mineralization. Our study show that the halogen contents and trace element concentrations of apatite and zircon may have significant potential to explore the difference in the nature of ore-forming magma between the porphyry Cu-Mo and Mo deposits.

## 2. Regional geological background

NE China is located within the east segment of the Central Asian Orogen Belt (CAOB; Fig. 1a), which lies between the Siberian and North China cratons (Jahn et al., 2000). The region is characterized by Phanerozoic crustal growth related to progressive subduction of the Paleo-Asia Ocean and amalgamation of a series of micro-continental massifs or terranes (Sengör and Natal'in, 1996; Pirajno and Santosh, 2014), including the Erguna, Xing'an, Songliao, and Jiamusi blocks from northwest to southeast (Wu et al., 2011; Fig. 1b), followed by the interaction with the Mongol-Okhotsk and Pacific oceanic plates (Chen et al., 2017b). The detailed process is, during the Paleozoic, the subduction and closure of the Paleo-Asian Ocean caused the collision of Erguna, Xing'an and Songliao blocks from the northwest to the southeast—that were separated by a series of northeast-trending faults (Fig. 1b; Ouyang et al., 2013). During the Mesozoic, this region was characterized by the evolution of the Paleo-Pacific Ocean in the east and the Mongol-Okhotsk Ocean to the northwest, resulting in widespread magmatism and the accretion of the Jiamusi Massif and Nadanhada Terrane in the easternmost area of NE China (Wu et al., 2011).

NE China is an important metallogenic province for Mo deposits (Zeng et al., 2013). In the past decade, >80 Mo (Mo-bearing) deposits have been discovered, resulting in it become the largest molybdenum mineralization region in China (Fig. 1; Shu et al., 2016; Chen et al., 2012, 2017b). Most of the Cu-Mo and Mo deposits are of porphyry type (Zeng et al., 2013), and they are generally formed in Mesozoic, post-dating the closure of the Paleo-Asia Ocean (Ouyang et al., 2013; Chen et al., 2017b). These include the giant-scale WS porphyry Cu-Mo, DHS and LM porphyry Mo deposits, and also contain the medium-scale JC porphyry Cu-Mo and FA porphyry Mo deposits. The detailed geological characteristics of the five representative porphyry Cu-Mo and Mo deposits in NE China are listed in Table 1.

## 3. Geological background and samples

### 3.1. Wunugetushan porphyry Cu-Mo deposit

The WS deposit (with Cu–Mo metal reserve of 849.7 Mt at an average grade of 0.46% Cu and 0.053% Mo) is situated 30 km south of Manzhouli (Fig. 1b; Chen et al., 2011). The ore minerals mainly comprise molybdenite, chalcopyrite and pyrite, and occur either as disseminated structure in altered rocks or veinlet structure in coarse veins. The mineralization in the WS district is associated with a monzogranite porphyry that has yielded SIMS zircon U-Pb ages 180.4 ± 1.4 Ma (Wang et al., 2015). Molybdenite Re-Os in the WS porphyry Cu-Mo deposit indicate that the ore-formation occurred at 180.5 ± 2.0 Ma, which is within analytical error of the age of the host monzogranite porphyry (Wang et al., 2015). The WS monzogranitic porphyry (WS granite) is reddish-brown with porphyritic texture, and are compose of quartz (20–25 vol%), plagioclase (15–18 vol%), K-feldspar (15–17 vol%), with minor amounts of biotite phenocrysts (~5 vol%). The groundmass (30–35 vol%) is composed of quartz, plagioclase, K-feldspar (Fig. 2a). Some quartz grains display distinct corroded irregular textures, and plagioclase in the groundmass is partly replaced by kaolinite and sericite. Most of biotite is altered to chlorite. The accessory minerals are mainly composed of apatite, zircon, and magnetite. Apatite grains from the WS granite are commonly occurs as individual crystals or euhedral inclusions enclosed in early-formed minerals (such as plagioclase and biotite). The Cu-Mo mineralization and associated magmatism in the WS area should generated by the southeastward subduction of the Mongol-Okhotsk oceanic plate beneath the Erguna Massif (Wang et al., 2015). In the Erguna block, geochemical data on the Mesozoic granitoids and mineralization associated rocks on southeastern part of Mongol-Okhotsk Orogen show an affinity with arc magmas, indicating an active continental margin related to the southward's subduction of the Mongol-Okhotsk oceanic plate (Chen et al., 2011; Wu et al., 2011; Xu et al., 2013a). In addition, paleomagnetic study of Late Jurassic volcanic activity in the Chengde area and Tiaojishan Formation, Yanshan Belt, North China, indicated that the Mongol-Okhotsk Ocean was still open at ca. 155 Ma (Pei et al., 2011; Ren et al., 2016). This result is consistent with reports by Dmitry et al. (2010) and Cogné et al. (2005), who proposed that the final closure of the Mongol-Okhotsk Ocean occurred in the Early Cretaceous in the Amur and Okhotsk sea area.

### 3.2. Jinchanggou porphyry Cu-Mo deposit

The JC porphyry Cu-Mo deposit is located in the 40 km southern of Jidong Country in the eastern Heilongjiang, NE China, and contains Cu and Mo reserves of >10 Kt with an average grade of 0.57% Cu and 0.16% Mo (Chen et al., 2010a). The ore minerals mainly comprise molybdenite, pyrite, pyrrhotite, sphalerite and chalcopyrite. The host granodiorite porphyry has a zircon U–Pb age of 114 ± 2.2 Ma (Sun et al.,

**Table 1**
Summary geological characteristics of five representative porphyry Cu-Mo and Mo deposits in NE China (according to Chen et al., 2017b).

| Deposit, province | Type | Size | Reserve @Grade | Molybdenite Re-Os | Related instrusion | Tectonic environment |
|---|---|---|---|---|---|---|
| Wunugetushan, Inter Mongolia | Porphyry Cu-Mo | G | 849.7 Mt @0.46% Cu;@ 0.055% Mo | 180.5 ± 2.0 Ma | Monzogranite porphyry | Subduction environment |
| Jinchanggou, Heilongjiang | Porphyry Cu-Mo | M | > 10 Kt @0.57% Cu; @0.16% Mo | 114 ± 2.2 Ma | Granodiorite porphyry | Subduction environment |
| Luming,Heilongjiang | Porphyry Mo | G | Mo: 890 Kt @0.088% | 177.9 ± 2.6 Ma | Monzogranite porphyry | Intra-continental environment |
| Fu'anpu Jilin | Porphyry Mo | M | Mo: 30 Kt @0.125% | 166.9 ± 6.7 Ma | Porphyritic monzogranite | Intra-continental environment |
| Daheishan, Jilin | Porphyry Mo | G | 1090 Kt @0.06% Mo; | 169.2 ± 1.2 Ma | Granodiorite porphyry | Intra-continental environment |

*Abbreviations*: For tonnage and size: Kt = 1000 t; G = giant (>500 Kt Mo); L = large (100–500 Kt Mo); M = medium (10–100 Kt Mo).

2012). The JC granodiorite porphyry (JC granite) is porphyritic and contains phenocrysts of quartz (25–30 vol%) and plagioclase (20–25 vol %) in a groundmass of plagioclase (15–18 vol%), quartz (10–12 vol%), K-feldspar (5–10 vol%) and biotite (2–5 vol%) (Fig. 2c). Quartz and plagioclase phenocrysts are euhedral, with an average diameter of 50–800 μm. Most of plagioclase in the matrix is altered to kaolinite and sericite. Biotite usually occurs as small, subhedral phase at the gaps between K-feldspar or quartz phenocrysts, and most of the biotite was replaced by chlorite. The accessory minerals include Fe-Ti oxides, apatite, and zircon. Apatite in JC granites have two types, altered and primary, and here the primary apatite was selected for study in this text. The primary apatite grains from the JC granite are commonly occurs as euhedral crystals, can be wrapped in K-feldspar and biotite. The Cu-Mo mineralization and associated magmatism in the JC area should generated by the northwestward subduction of the Paleo-Pacific oceanic plate. Firstly, Wu et al. (2011) proposed that Eastern China is mainly affected by circum-Pacific tectonics, and since the Early Jurassic NE China has been strongly influenced by the westward subduction of the paleo-Pacific plate. Petro-geochemical characteristics indicate that the existence of voluminous late Early Cretaceous calc-alkaline volcanic rocks in Ji-Hei area formed in an active continental-margin setting and was induced by the subduction of the Paleo-Pacific Plate beneath the Eurasian continent (Yu et al., 2009; Wu et al., 2011; Xu et al., 2013b). Secondly, numerous porphyry Cu-Au and epithermal Au deposits closed to the JC porphyry Cu-Mo deposit (i.e., Jinchang, xiaoxi'nancha, Jiusangou, Duhuangling, Naozhi, Nongping and Wuxinghsan gold deposits) during this episode (ca. 129 and 95 Ma) are mainly concentrated in the in eastern Jilin and Heilongjiang provinces, and they are dominated by typical of arc-related magmatic-hydrothermal and hydrothermal ore deposits (Han et al., 2012; Xu et al., 2013a, 2013b; Cai et al., 2019).

### 3.3. Luming porphyry Mo deposit

The LM porphyry Mo deposit located 45 km northeast of Tieli city (Fig. 1b), and it has proven Mo reserves of 890 Kt with an average grade of 0.088% Mo (Shi et al., 2007). The ore minerals are dominated by molybdenite, pyrite, pyrrhotite, chalcopyrite, and hematite with minor molybdite, limonite, covellite and bornite (Cheng et al., 2015). The host monzogranite porphyry has a zircon U–Pb age of 176 ± 2 Ma (Yang et al., 2012), which is consistent with molybdenite Re-Os isochron age of 177.9 ± 2.6 Ma (Hu et al., 2014). The LM monzogranitic porphyry (LM granite) is dark-gray in color and contains phenocrysts of quartz (15–17 vol%), plagioclase (15–20 vol%) and K-feldspar (15–20 vol%) in a groundmass of plagioclase (10–15 vol%), K-feldspar (5–10 vol%), quartz (5–10 vol%), and biotite (5–8 vol%) (Fig. 2e). Anhedral quartz, together with biotite, occur intergranular phases along the boundary of K-feldspar and quartz phenocrysts. The accessory minerals include, titanite, apatite, zircon and magnetite. Apatite grains from the LM granite are commonly intergrown with plagioclase, K-feldspar and quartz, and occur as euhedral and hexagonal prismatic crystals (Fig. 2e). Tan et al. (2012) suggested that the LM porphyry Mo deposit was formed in a post-collisional extension setting. Yang et al. (2012) proposed that the formation of LM porphyry Mo deposit is probably related to the subduction of Paleo-Pacific plate and the amalgamation between Jiamusi and Songnen massifs in the Jurassic. Cheng et al. (2015) and Chen and Zhang (2018) reported that the host monzogranite porphyry may be derived from partial melting of juvenile crust which formed in Middle-Late Proterozoic, and is probably related to the subduction of Paleo-Pacific plate.

### 3.4. Fu'anpu porphyry Mo deposit

The FA porphyry Mo deposit is located ~26 km east of Shulan City in Jilin Province (Fig. 1b), with Mo reserves of 30 Kt, and with an average grade of 0.04–0.16% (Li et al., 2009). The host rocks consist of porphyritic monzogranite, in which nine ore bodies have been discovered (Zhang, 2013). Molybdenite Re-Os and zircon U-Pb dating of the host porphyritic monzogranite in the FA porphyry Mo deposit indicate that the ore-formation and host porphyry emplacement occurred at 166.9 ± 6.7 Ma and 167.1 ± 0.8 Ma, respectively (Li et al., 2009; Zhang, 2013). The FA porphyritic monzogranite (FA granite) is light-gray in color with porphyritic texture. It comprises phenocrysts K-feldspar (10–15 vol%), quartz (25–30 vol%), plagioclase (10–15 vol%), and the groundmass (35–40 vol%) is composed of K-feldspar, quartz, and biotite (Fig. 2g). K-feldspar rims and plagioclase are partially replaced by sericite. The accessory minerals include apatite, Fe-Ti oxides, and zircon. Apatite grains are commonly intergrown with plagioclase, K-feldspar and biotite, and occur as euhedral prismatic crystals (Fig. 2g). The porphyritic monzogranite associated with the Mo deposits have relatively depleted mantle-like Nd and Hf isotopic compositions, suggesting that the ore-forming granitic magma may have predominantly been derived from juvenile lower crust material (Hou, 2017).

### 3.5. Daheishan porphyry Mo deposit

The DHS porphyry Mo deposit is located in the southern Lesser Xing'an-Zhangguangcai Ranges and tectonically in the northwestern Songliao Block, Jilin Province (Fig. 1b). Recently, a total Mo metal reserve of 1090 Kt with an average Mo grade of 0.06% was reported, and mineralization is closely related to the small (~0.46 $km^2$) Qiancuoluo granodioritic porphyry intrusion (Zhou et al., 2015). The ore minerals are predominantly molybdenite and pyrite, and consist minor sphalerite and chalcopyrite. The molybdenite yielded a Re–Os isochron age of 169.2 ± 1.2 Ma (Zheng and Yu, 2017) which is indistinguishable from the host Qiancuoluo granodioritic porphyry age (169.6 ± 0.4 Ma, Zhou et al., 2014). The DHS granodioritic porphyry (DHS granite) is greyish white with porphyritic texture, and are composed of quartz (20–25 vol %), plagioclase (15–20 vol%), K-feldspar (10–15 vol%), and biotite (~5 vol%) phenocrysts. The groundmass (40–45 vol%) is composed of fine-grained quartz, plagioclase, K-feldspar and biotite. Plagioclase is mostly

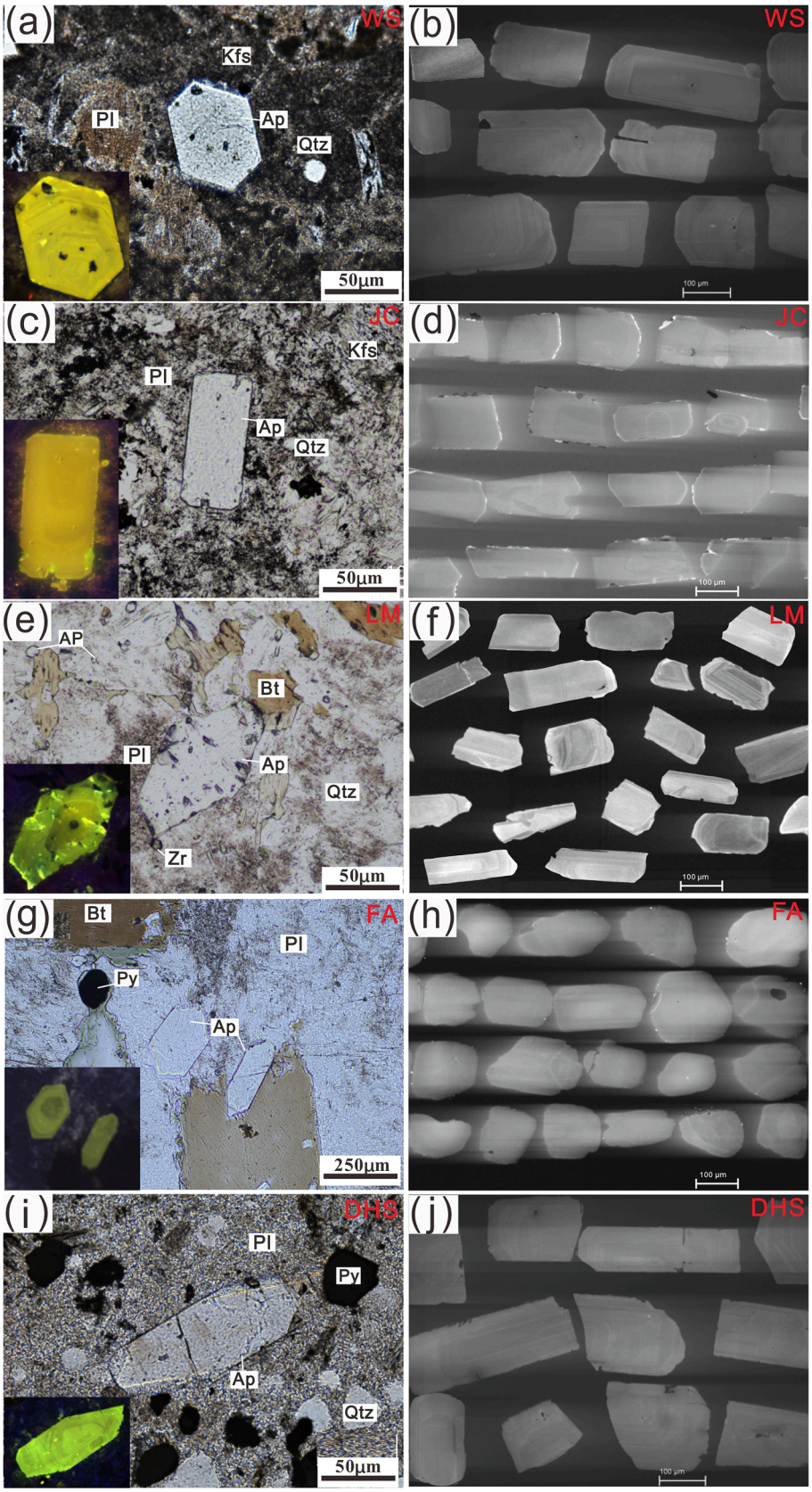


**Fig. 2.** Petrography and cathodoluminescence (CL) images showing examples of typical mineral assemblages and the occurrence of apatite grains in representative granites associated with five porphyry Cu-Mo and Mo deposits. WS: Wunugetushan porphyry Cu-Mo deposit; JC: Jinchanggou porphyry Cu-Mo deposit; LM: Luming porphyry Mo deposit; FA: Fu'anpu porphyry Mo deposit; DHS: Daheishan porphyry Mo deposit. Mineral abbreviations: Qtz = quartz, Kfs = K-feldspar, Pl = plagioclase, Bt = biotite, Ap = apatite, Zr = zircon, Py = Pyrite. Mineral symbols are after Whitney and Evans (2010).

altered to kaolinite and sericite. Most biotite is altered to chlorite. The accessory minerals are mainly composed of apatite, titanite, zircon, and magnetite. Apatite occurs as euhedral hexagonal grains intergrown with plagioclase, biotite and some feldspar (Fig. 2i). Chen et al. (2017b) consider that the DHS porphyry Mo deposit was originated from partial melting of a thickened young lower crust during post-collisional extension, which is definitely compatible with the geological context in the area.

## 4. Analytical methods

### 4.1. Sample preparation

The least altered representative ore-related granites from five porphyry Cu-Mo and Mo deposits were used for petrographic studies and apatite chemical analyses. All these samples were made into thin sections for petrographic study and one sample was taken from each stock to separate apatite and zircon. The apatite and zircon grains were separated from the samples by using standard heavy liquid and magnetic methods, and then hand-picked under the microscope. The selected grains were mounted in epoxy blocks and polished. Before the analysis, the apatite and zircon grains were examined using transmitted/reflected light microscopy and CL to determine their internal textures. Apatites from the representative granites are euhedral or hexagonal and show a magmatic texture with clear oscillatory zoning in CL images (Fig. 2b, d, f, h, and j), indicates that they are primary magmatic origin and have undergone negligible alteration. The paragenetic relationship between apatite and phenocryst implies that apatite crystallizes early within the parental magmas of these porphyries. Therefore, the chemical composition of the selected apatite crystals could effectively reflect the information of parental magmas. Zircons from the representative granites are also euhedral and prismatic shape. They are transparent in transmitted light and show fine-scale, well-developed bright oscillatory zoning in the CL images.

### 4.2. Whole-rock major and trace elements

The least altered samples were powdered to ~200-mesh size for geochemical analyses. The major elements of the whole rock were determined using a Rigaku RIX 2000 X-ray fluorescence (XRF) spectrometer at the State Key Laboratory of Isotope Geochemistry, Guangzhou Institute of Geochemistry, Chinese Academy of Sciences (SKLIG, GIGCAS). The trace elements were analyzed using an inductively coupled plasma mass spectrometer (ICP-MS) at the SKLIG, GIGCAS. The detailed analytical procedures are described by Li et al. (2000). An internal standard solution containing Rh was used to monitor the signal drift during counting. A set of USGS and Chinese national rock standards, including GSR-1, GSR-2 and GSR-3, were chosen for calibration. The analytical precision is typically better than 5%.

### 4.3. Apatite major and trace element analysis

Major element compositions of apatite were examined using electron microprobe analysis (EMPA) and a JEOL JXA 8230 electron microprobe at the KLMM, GIGCAS. The analytical conditions for the EMPA of apatite were as follows: 15 kV accelerating voltage, 20nA beam current, and 5 μm beam diameter. The peak and background counting times were 20 and 10 s for Ca and P, 10 and 5 s for F and Cl, and 60 and 30 s for Si and S. The Kα line was chosen for the analysis of all elements. The elements F and Cl were analyzed first to minimize their loss. The analytical results were reduced using ZAF correction. The used standards were fluorapatite for Ca and P, $BaF_2$ for F, tugtupite for Cl, and diopside for Si. The relative precisions were ±2% for Ca, P, and F and ±5% for Si and Cl.

Trace element concentrations of apatite were measured with *in situ* LA-ICP-MS at the KLMM, GIGCAS, using an Agilent 7900a ICP-MS equipped with a Resonetic 193 nm ArF excimer laser ablation system. The *in situ* LA-ICP-MS analyses of apatite were performed on the same sample spots that were used for EMPA. The operating conditions were: 80 mJ laser energy, 8 Hz ablation frequency, and 43 μm laser ablation spot diameter. The CaO content determined by EMPA was used as an internal standard for the apatite data calibration using ICP-MSDataCal (Liu et al., 2010). The LA-ICP-MS detection limit was below 0.1 ppm and the analytical uncertainty was better than 10% (relative percentage) for most of the analyzed elements. All analysis spots were carefully selected to avoid mineral and melt inclusions and cracks. The detailed analytical condition for the EMPA of apatite is described in Qu et al. (2019).

### 4.4. Apatite Sr and Nd isotope analysis

In situ Sr isotope analysis for apatite was conducted using the RESOlution laser ablation system coupled to Nu Plasma II multi-collector (MC) ICP-MS at the State Key Laboratory of Geological Processes and Mineral Resources, China University of Geosciences (Wuhan). Analyses were carried out using a spot size of 108 μm with a repetition rate of 10 Hz and an energy density of ~3–5 J/cm$^2$. Every 5 to 7 sample analyses were bracketed by an analysis of an in-house coral standard as the external standard to check the analytical reliability and stability. The measurements involved correction of spectral interferences for Kr, Rb, and doubly charged REE as described in Chen and Simonetti (2014). The average $^{87}Sr/^{86}Sr$ isotopic composition obtained for the coral standard is 0.70916 ± 0.00004 (2σ, n = 30), which is consistent with the recommended value of 0.70910 ± 0.00002 as determined by ID-TIMS analyses (Bizzarro et al., 2003).

All *in situ* apatite Nd isotope analyses were performed with a Neptune Plus MC-ICP-MS (Thermo Scientific) coupled with a Resolution M-50 193 nm laser ablation system (Resonetics) at the SKLIG, GIGCAS. The detailed description of the two instruments can be found in Zhang et al. (2014) and the detailed data reduction procedure can be found in Zhang et al. (2015). The 40 analyses of McClure apatite and 25 analyses of Durango apatite performed in this study yielded weighted means of $^{143}Nd/^{144}Nd$ = 0.512280 ± 0.000055 (2SD) and $^{143}Nd/^{144}Nd$ = 0.512470 ± 0.000060 (2SD), respectively, which are consistent (within errors) with the value reported in Yang et al. (2014).

### 4.5. Zircon trace element and Hf isotope analyses

The zircon trace element analyses and U–Pb dating using an Agilent 7900a (ICP-MS) equipped with a 193 nm laser system at the Key Laboratory of Mineralogy and Metallogeny (KLMM), GIGCAS. The analyses were performed at a constant energy of 80 mJ using a spot diameter of 31 μm and repetition rate of 8 Hz. The standard zircon 91,500 and NIST glass 610 (Pearce et al., 1997) were used for the external calibration of the U–Pb dating and trace element analyses, respectively. As the internal standard for the trace element concentrations, $^{29}Si$ was used. Details about the operating conditions and data processing are described in Tu et al. (2011). The zircon isotope ratios and trace element contents were calculated using ICPMSDataCal (Liu et al., 2010). The analytical data were reduced, calculated, and plotted using the ISOPLOT software (Ludwig, 2003).

In situ zircon Hf isotopic analyses were performed on a Neptune Plus MC-ICP-MS (Thermo Scientific) coupled with a Resolution M-50 193 nm laser ablation system (Resonetics) at the SKLIG, GIGCAS. The detailed description of the two instruments can be found in Zhang et al. (2014). The laser parameters were as follows: beam diameter of 45 μm, repetition rate of 6 Hz, and energy density of ~4 J cm$^{-2}$. The detailed data reduction procedure is reported in Qu et al. (2019).

## 5. Results

### 5.1. Whole-rock major and trace element geochemical compositions

Major and trace element compositions of representative ore-related granites from the study area are listed in Supplementary Table 1. Almost all of the ore-related granites in this area have 64.30–74.21 wt% $SiO_2$ (recalculated to 100% without LOI) and show a relatively high concentrations of $K_2O$ (Fig. 3a), with most of data plotting in the field of high-K calc-alkaline series but JC samples plotting in the field of the shoshonite series (Fig. 3b). This is due to the JC samples have high loss in ignition (LOI) assays of 4.47–7.02 wt%, indicating that they have undergone significant alteration (Supplementary Table 1). These samples have $P_2O_5$ concentrations that negatively correlate with $SiO_2$ concentrations, a feature that is typical of I-type rocks (Supplementary Table 1; Li et al., 2007). In chondrite-normalized rare earth element diagrams, all the samples show enrichment of LREEs and depletion of HREEs (Fig. 3c). They are moderately fractionated, yielding LREE/HREE ratios of 9.50–19.6 and $(La/Yb)_N$ ratios of 10.7–32.2 (Supplementary Table 1). In primitive mantle-normalized diagrams (Fig. 3d), these granites have arc affinity with enrichment in large ion lithophile elements (LILEs), including K, Rb, Ba, Pb, and Sr, and depletions in high field strength elements (HFSEs) including Nb, Ta, Th, Zr, Ti, and P. It is worth noting that these granites from porphyry Cu-Mo and Mo deposits have slightly different Th, Ba, Nb, La and Yb contents, plus different Ba/La, Th/Yb, Ba/Th and Th/Nb ratios (Fig. 8). Temperature estimation by using zircon saturation thermometer (Watson and Harrison, 1983) indicates that the WS and JC granites have relatively lower whole rock zircon saturation temperatures (746–787 °C) than those from the LM, FA and DHS granites (781–814 °C; Supplementary Table 1).

### 5.2. Apatite geochemistry

Major and trace element compositions of apatite are presented in Supplementary Table 2 and Fig. 7. The OH content in apatite is calculated by stoichiometry based on 8 anions and assuming that the halogen site is fully occupied with $X_{F\text{-}ap} + X_{Cl\text{-}ap} + X_{OH\text{-}ap} = 1$, where X = mole fractions modal of F, Cl and OH (Piccoli and Candela, 2002). Most apatites have CaO content in the range of 53.02 to 56.85 wt%, and $P_2O_5$ in the range of 41.13 to 43.01 wt%. Apatite from the WS and JC granites contain less F (1.27–2.26 wt%) but more Cl (0.11–0.48 wt%) contents than those from the LM, FA and DHS granites (F = 2.23–4.45 wt% and Cl = 0–0.10 wt%, respectively; Fig. 7c). The calculated OH contents of apatites from the WS and JC granites (0.38–0.60 apfu) are clearly higher than those from the LM, FA and DHS granites (0–0.37 apfu; Fig. 7a). All the apatites from the representative granites exhibit fairly a right inclined distribution pattern with enrichment of LREE comparative to HREE (Fig. 4). The apatites from the WS and JC granites have relatively higher Ba (0.74–3.79 ppm) and Sr (458–761 ppm) contents than those from the LM, FA and DHS granites (Ba = 0–1.39 ppm, Sr = 105–570 ppm; Fig. 7d).

In situ Sr and Nd isotopic compositions of the apatites from the representative granites are listed in Supplementary Table 3 and plotted in Fig. 6a, b. Due to high Sr (>105 ppm) and essentially negligible Rb (<2.56 ppm) concentrations in the analyzed apatite (Supplementary Table 3), therefore the present-day $^{87}Sr/^{86}Sr$ ratios of the grains can be considered as the initial Sr isotopic signatures. The apatites from these granitic rocks exhibits fairly homogenous $(^{87}Sr/^{86}Sr)_i$ and εNd(t)

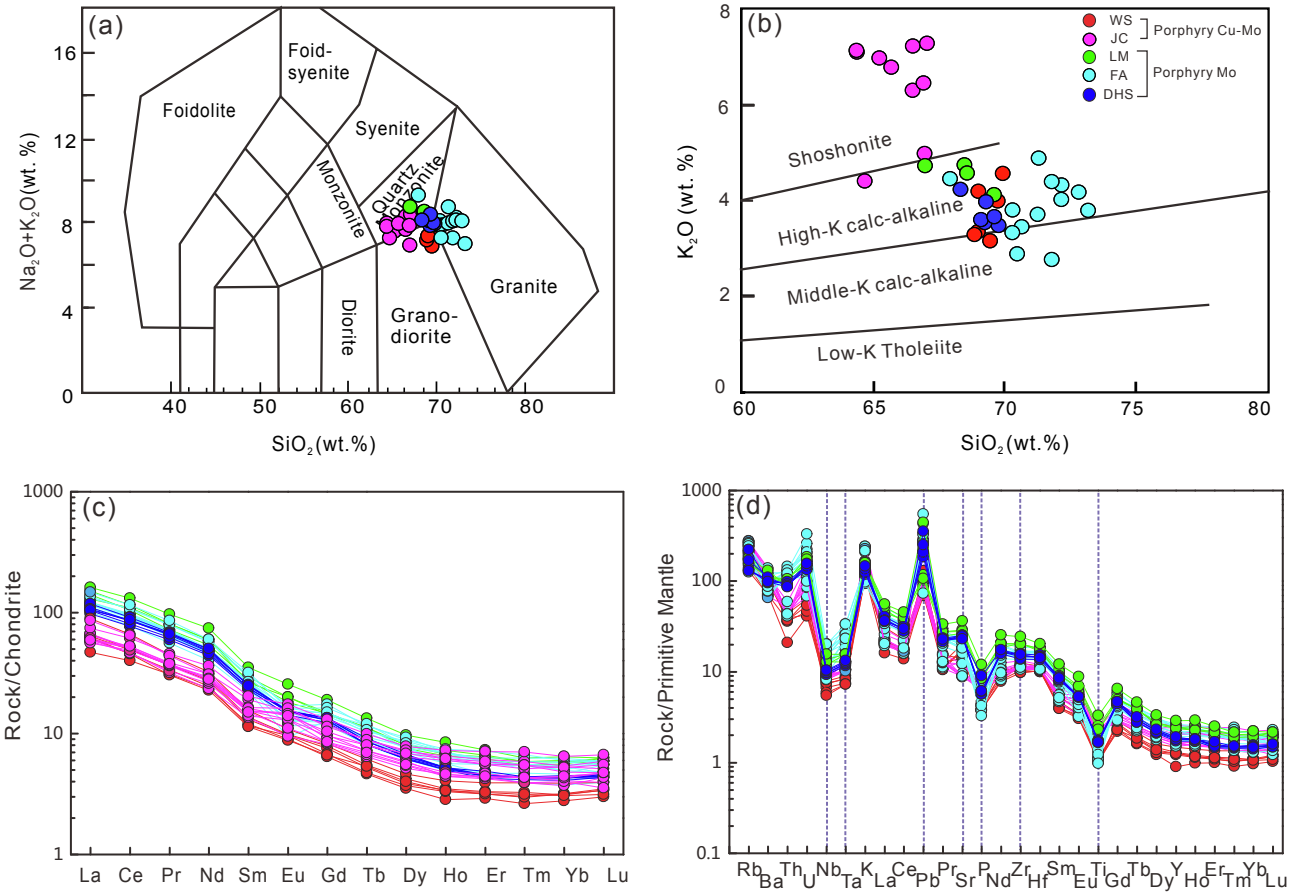


**Fig. 3.** Diagrams showing variations in the composition of representative granitic rocks from the northeastern China. (a) $Na_2O + K_2O$ vs. $SiO_2$ diagram (after Middlemost, 1994); (b) $K_2O$ vs. $SiO_2$ (after Peccerillo and Taylor, 1976); (c) Chondrite-normalized REE patterns and (d) primitive mantle-normalized spider diagrams of the representative granites from five porphyry Cu-Mo and Mo deposits (Normalizing values are taken from Sun and McDonough, 1989).

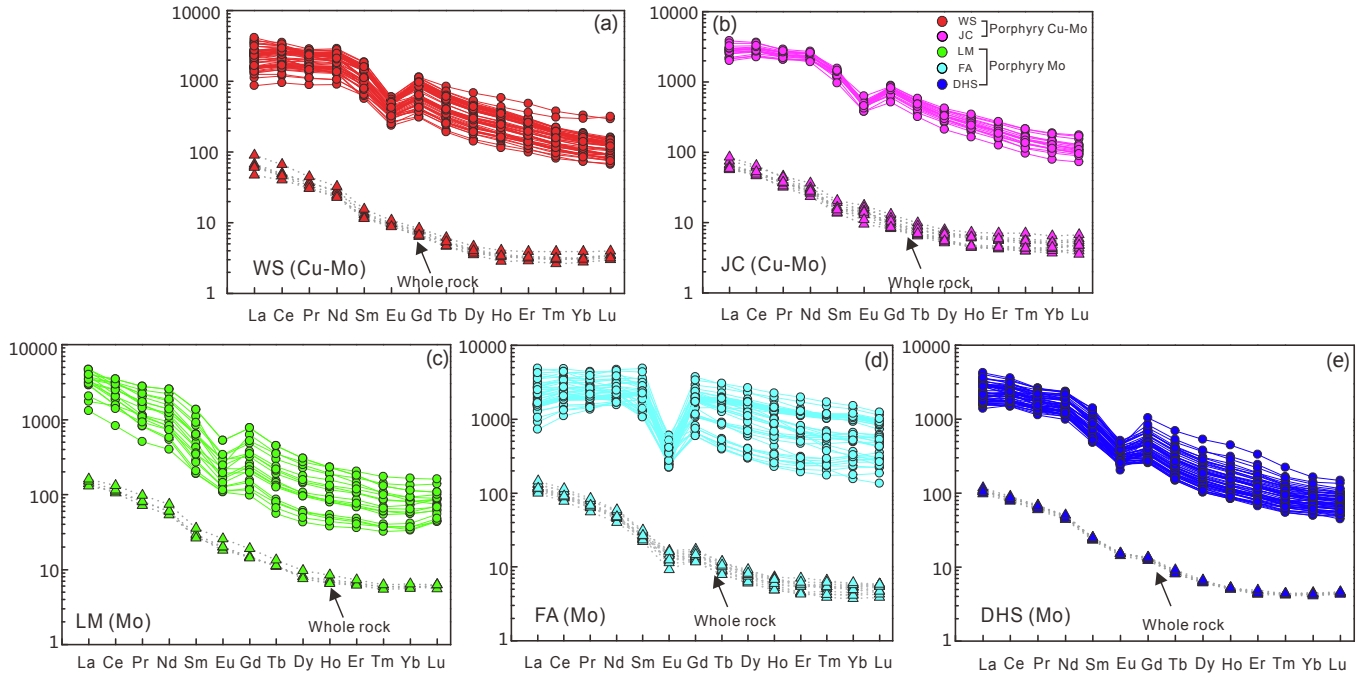


**Fig. 4.** Chondrite-normalized REE patterns for apatite (colored symbols with colored lines) and their granitic host rocks (colored symbols with dashed lines) associated with Cu-Mo and Mo mineralization in NE China. Chondrite-normalized values are from Sun and McDonough (1989). Abbreviations of deposits: WS, Wunugetushan; JC, Jinchanggou; LM, Luming; FA, Fu'anpu; DHS, Daheishan.

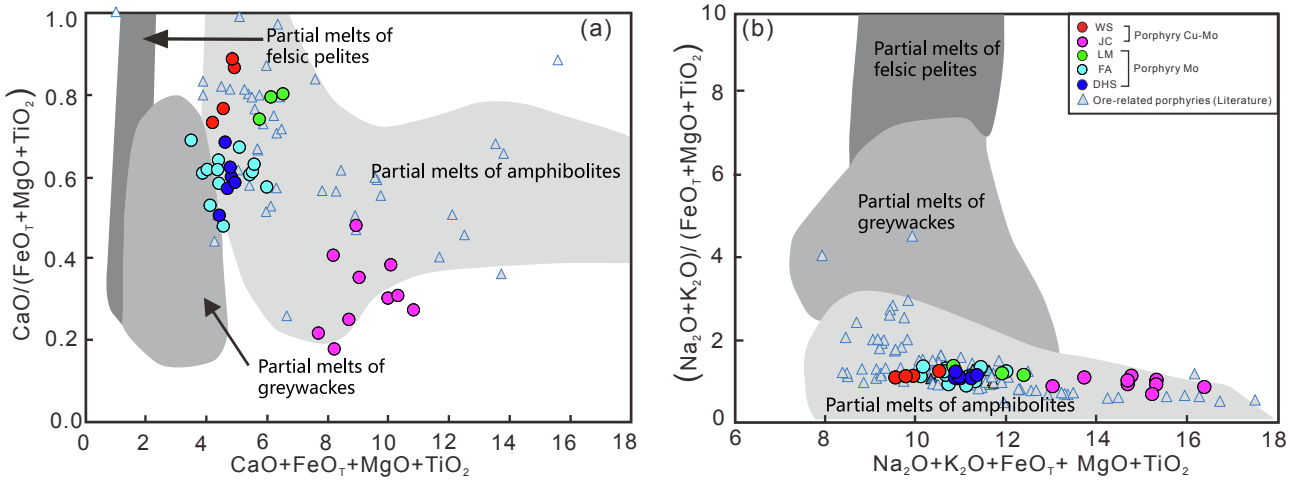


**Fig. 5.** Compositional fields of experimental melts derived from melting of felsic pelites, metagreywacke and amphibolites in diagram of (a) CaO/(FeO$^T$ + MgO + TiO$_2$) vs. (CaO + FeO$^T$ + MgO + TiO$_2$) (b) (Na$_2$O + K$_2$O)/(FeO$^T$ + MgO + TiO$_2$) vs. (Na$_2$O + K$_2$O + CaO + FeO$^T$ + MgO + TiO$_2$) (after Patiño Douce, 1999). The whole rock data source is taken from our data (Supplementary Table 1), and from Taipingchuan (Chen et al., 2010b), Huzhagaitu (Liu, 2016), Sankuanggou (Deng et al., 2018), Huojihe (Hu et al., 2019), Cuiling (Yang et al., 2012), Chang'anbu, Jidetun (Ju et al., 2019), Xinhualong (Sun et al., 2012), Baoshan, Jiapigou, Kanyuangou (Hou, 2017), and Houdaomu Mo deposits (Zhang, 2013).

isotopic compositions. The $(^{87}Sr/^{86}Sr)_i$ ratios of apatites from the representative granites ranging from 0.704092 to 0.707573 (Supplementary Table 3 and Fig. 6a). The εNd(t) and $^{143}Nd/^{144}Nd$ ratios of the apatites from these granitic rocks are −4.24 to 3.52 and 0.512300–0.512764, respectively, corresponding to the two-stage Nd model age range between 610 and 1306 Ma (most in the range of 756–1020 Ma; Fig. 6b).

### 5.3. Zircon geochemistry

Zircon trace element and Hf isotopic compositions from the representative granites are listed in Supplementary Tables 4 and 5, respectively. All of the zircons obtained from the representative granites within NE China are euhedral with clear oscillatory zoning in CL images and moderate to high Th/U values (0.35–1.00; Supplementary Table 4), indicating that they are primary magmatic grains that have not undergone significant alteration. The zircon crystals from the WS and JC granites have higher (Ce/Nd)/Y and lower Dy/Yb ratios than those from the LM, FA and DHS granites in Fig. 7b, but they share similar Hf isotopic compositions (Fig. 6c). These zircons yield $^{176}Hf/^{177}Hf$ ratios from 0.282623 to 0.283052 and εHf(t) values from −1.5 to 13.5 (Fig. 6c), corresponding to two-stage $T_{DM2}$ model ages range between 354 and 1317 Ma (most in the range of 505–918 Ma), in good agreement with the apatite two-stage Nd model ages.

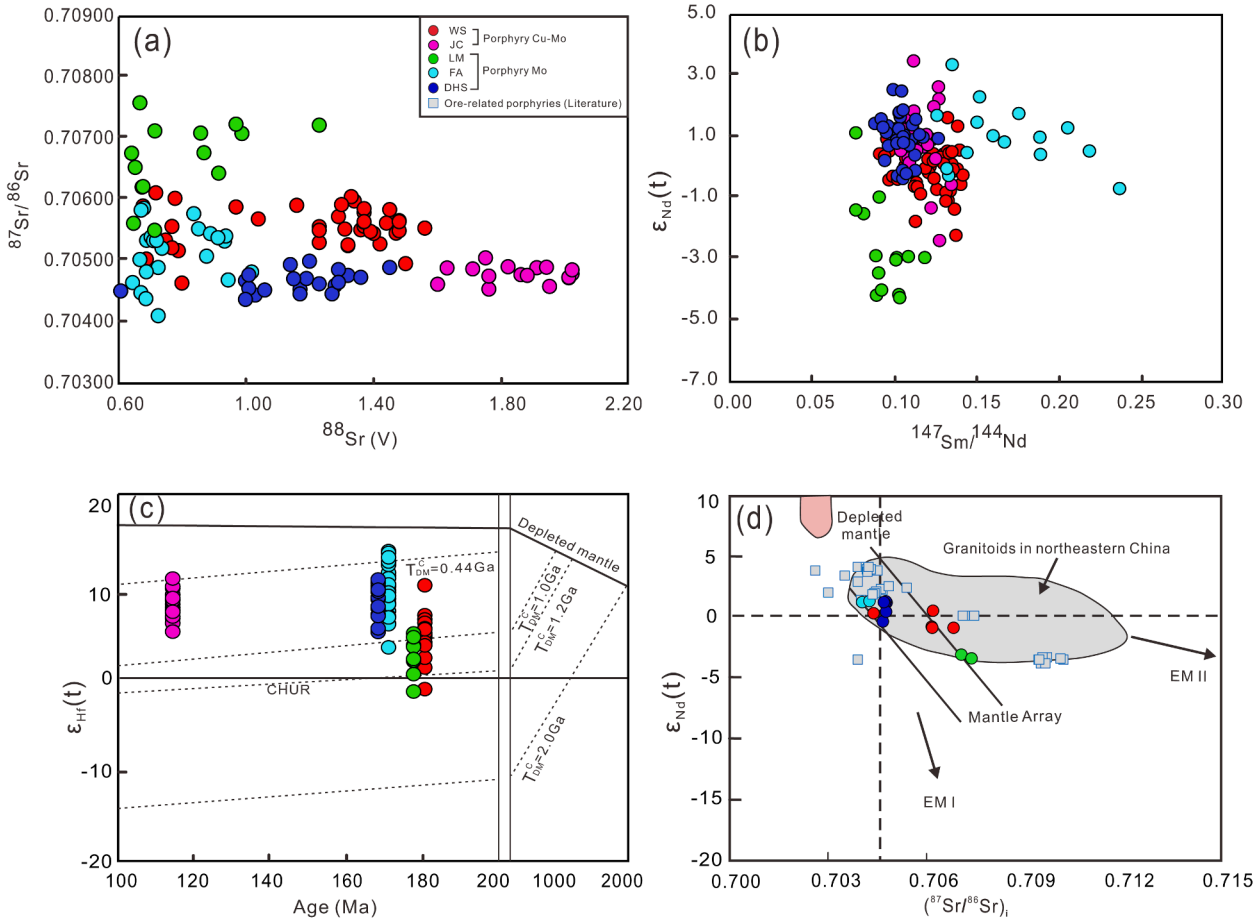


**Fig. 6.** (a) Plots of $(^{87}Sr/^{86}Sr)_i$ ratios versus $^{88}Sr$ (v) values (b) $^{143}Nd/^{144}Nd$–εNd(t) in the apatite from these porphyry Cu-Mo and Mo deposits. (c) Plot of εHf(t) vs. U-Pb age (Ma) of zircon from these porphyry Cu-Mo and Mo deposits. (d) Plot of εNd(t) vs. $(^{87}Sr/^{86}Sr)_i$ for whole-rock samples from the five porphyry Cu-Mo and Mo deposits and several other porphyry Mo-bearing deposits in the Xing'an Range region. The complied whole-rock Sr-Nd isotopic compositions of porphyry Mo deposits include Xinhualong (Sun et al., 2012), Huojihe (Hu et al., 2019), Taipingchuan (Chen et al., 2010b), Diyanqinamu (Sun et al., 2014), Dongbulage (Guo et al., 2020), Sankuanggou (Deng et al., 2018), Dashihe, Houdaomu, and Jidetun (Zhang, 2013). The shaded area of the granitoids in NE China is from Wu et al. (2003).

## 6. Discussion

### 6.1. Nature of magmatic source of the porphyry Cu-Mo and Mo deposits

Almost all the ore-related representative granites from these porphyry Cu-Mo and Mo deposits belong to high-K calc-alkaline I-type granite (Supplementary Table 1). Whole rock zircon saturation temperatures of these granitic rocks with 746–814 °C (Supplementary Table 1), which are lower than the temperatures of typical A-type granites (>900 °C; King et al., 1997). There are series of similar affinities of geochemistry and isotopes, indicative of a possible of homologous source for the WS, JC, LM, FA and DHS granites. Firstly, samples from these granites have Nb/Ta (7.88–17.36, average value of 12.9) and Zr/Hf values (34.0–44.4, average value of 37.4), which are similar to the crustal values (11.4 and 33, respectively; Supplementary Table 1; Taylor and McLennan, 1985). These granites also have low Ti/Zr ratios (7.46–22.6, average value of 13.7), which are consistent with those of typical crustal rocks (Ti/Zr < 30; Hans Wedepohl, 1995). Secondly, in the source region discrimination diagram (Fig. 5), all samples plot into the fields of partial melting of amphibolite, together indicating the comparable magma source (Patiño Douce, 1999). Thirdly, these granites in this study have similar apatite $(^{87}Sr/^{86}Sr)_i$ ratios (0.704092 to 0.707573) and $\varepsilon_{Nd}(t)$ values (−4.24 to +3.52; Fig. 6a, b), which resemble the numerous Mesozoic granitoids in NE China with positive εNd (t) values (0 to +4) and low $(^{87}Sr/^{86}Sr)_i$ ratios (0.705 ± 0.001) (Jahn et al., 2000), all demonstrating a significant contribution from juvenile lower crust material. This interpretation is also supported by bulk-rock Sr-Nd isotopic data for these granites (Fig. 6d). The Sr-Nd isotopic compositions of the WS, LM, FA and DHS granites are consistent with those from many other ore-related granites from the Jurassic porphyry Mo deposits in the Great and Lesser Xing'an Range region (e.g., Taipingchuan, Honghuaerji, Diyanqinamu, Dongbulage, Huojihe, Cuiling, Liushengdian, Xinhualong, Changanbao, Dashihe and Houdaomu porphyry Mo deposits) and Mesozoic granitoids in NE China (Fig. 6d), together indicating that these granites most likely originated from relatively juvenile crust-derived melts. Fourthly, the zircon εHf(t) values (−1.5 to 13.5) of these granites almost all fall within the field between the chondrite uniform reservoir and depleted mantle, with a uniform $T_{DM2}$ age range of 354–1212 Ma (most in the range of 505–918 Ma; Fig. 6c), which are consistent with zircon εHf (t) values from the other Phanerozoic igneous rocks in the east CAOB (Yang et al., 2006), implying that they most likely formed via partial melting of juvenile crust (Qu et al., 2019). This has also been confirmed in this study that Mo is associated with magmas melted from juvenile crust materials (e.g., Farmer and DePaolo, 1984; Klemm et al., 2008).

In light of the discussion above, the whole-rock geochemistry and in-situ apatite Sr-Nd and zircon Hf isotopic compositions from the WS, JC, LM, FA and DHS granites in NE China suggest that they are originated from partial melting of a juvenile crustal source.

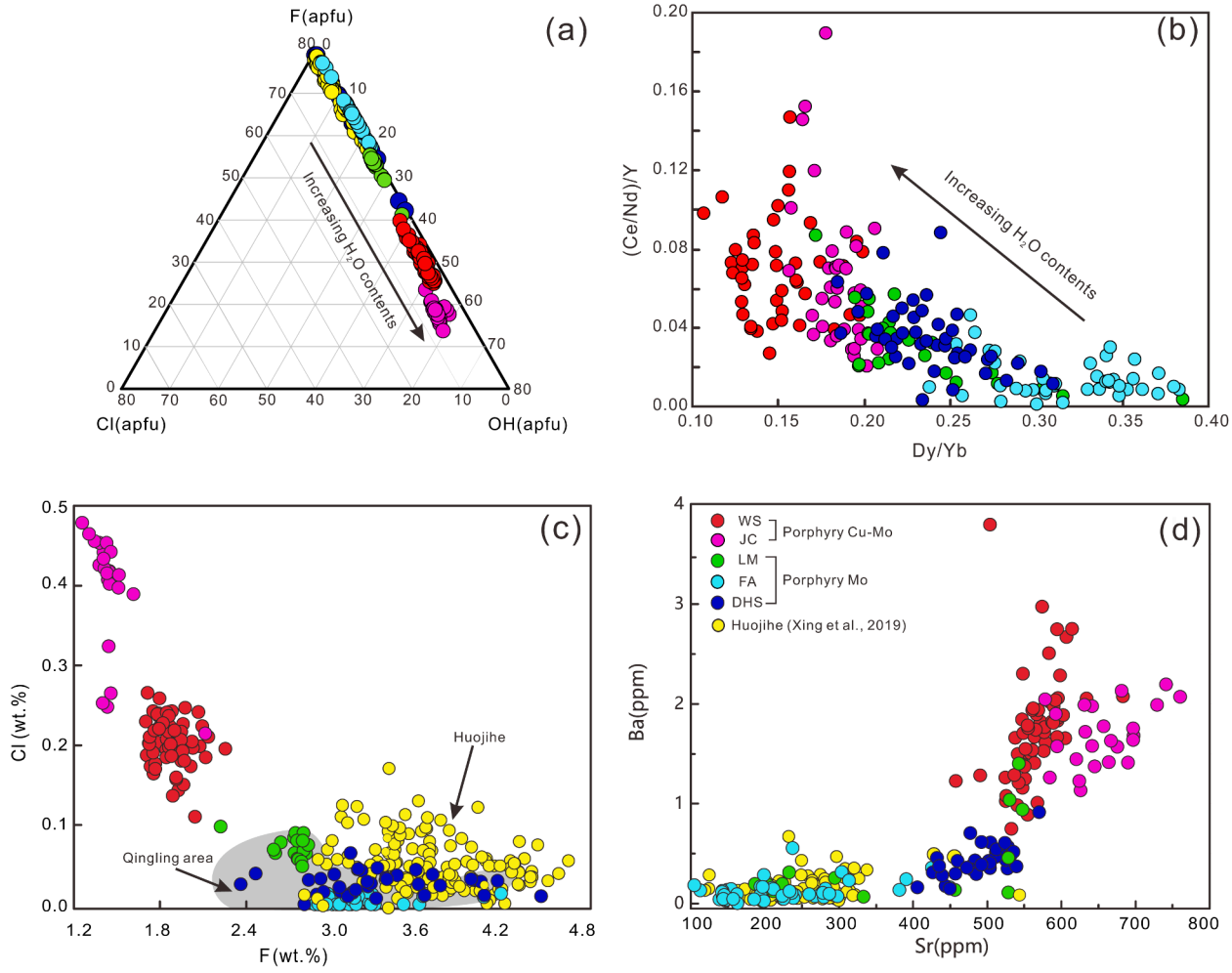


**Fig. 7.** Variation diagrams of major and trace element contents for apatite (a, c, d) and zircon (b) from the porphyry Cu-Mo and Mo deposits in NE China. (a) F-Cl-OH ternary diagram based on the F-Cl-OH atomic proportions in apatites; (b) variation diagrams of zircon (Ce/Nd)/Y vs. Dy/Yb ratios; (c) Cl (wt%) vs. F (wt%) in apatites; (d) Ba (ppm) vs. Sr (ppm) in apatites. The yellow circles represent apatite compositions of the granitoids from the Huojihe porphyry Mo deposit (Xing et al., 2019). The apatite data source in the Qinling area are taken from Yaochong (Mi et al., 2017), Jinducheng (Li, 2013), Nannihu, Shangfanggou, Shibaogou, and Yuku (Du et al., 2019), Sandaozhuang, Nantai, and Qiushuwan porphyry Mo deposits (Chen et al., 2017a).

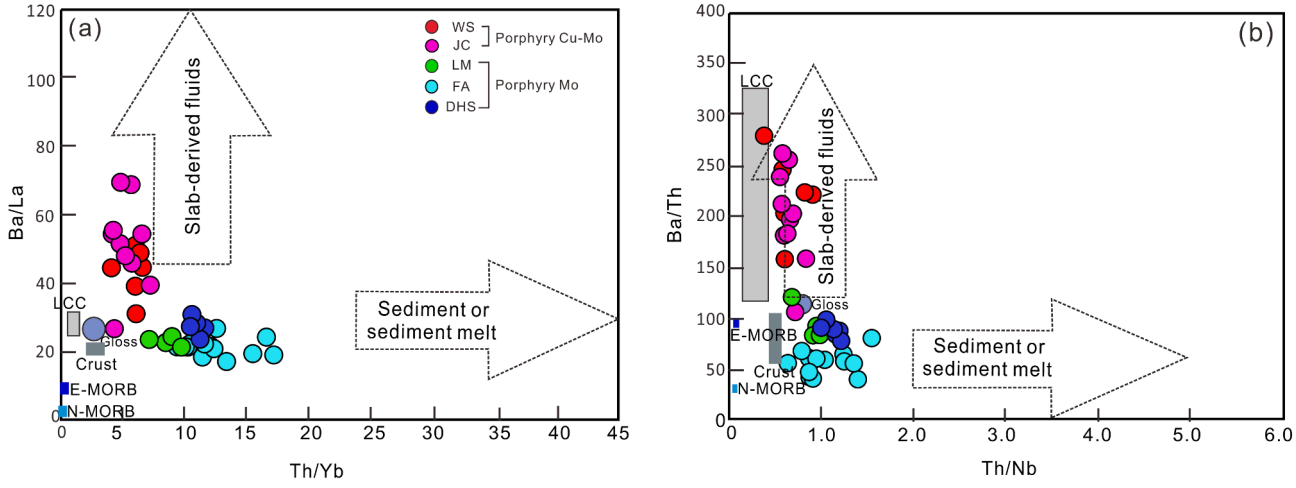


**Fig. 8.** (a) Ba/La vs. Th/Yb and (b) Ba/Th vs. Th/Nb diagram of the representative granites from these porphyry Cu-Mo and Mo deposits in NE China (after Xu et al., 2016).

### 6.2. Difference in nature of ore-forming magma of the porphyry Cu-Mo and Mo deposits

Generally, the LILEs (e.g., Rb, Ba, Sr, and K) and other fluid-mobile elements such as U and Pb are relatively mobile in fluids released from the subducted slab, whereas Th, LREEs and HFSEs are thought to be mobilized by the melts (Elliott et al., 1997). Consequently, high Ba/La, Ba/Th, Rb/Y, Sr/Th, and Sr/Nd ratios are generally thought to be indicative of arc magma derived from sources that input of slab-released fluids, whereas rocks with sources that had been enriched by partial melts derived from sediments are likely to have high Th/Yb, Th/Pb, and Th/Nb ratios (e.g., Zheng et al., 2011; Labanieh et al., 2012). The WS and JC granites near to the subduction zone have variable Ba/La and Ba/Th ratios, but narrow ranges of Th/Yb and Th/Nb ratios, indicating that their source were modified mainly by subducted slab-derived fluids (Fig. 8; e.g., Dokuz et al., 2020; Wu et al., 2016). Additionally, the ability of Cl-bearing hydrothermal fluids to transport Sr is well documented by field and experimental studies (La Cruz et al., 2019). As shown in Fig. 7d, the apatites from the WS and JC granites near to the subduction zone have higher fluid-mobile element Ba and Sr contents than those from the LM, FA and DHS granites, also suggesting that the magmatic source of porphyry Cu-Mo deposits were modified by subducted slab-derived fluids (e.g., Richards, 2015; Chen and Wu, 2020). In contrast, the LM, FA and DHS granites away from the subduction zone with lower Th/Yb and Th/Nb ratios, and narrow ranges of Ba/La and Ba/Th ratios, reflecting their derivation magma neither associated with enrichment sediments nor modified by slab-derived fluids (Fig. 8; Wu et al., 2016).

Volatile fluids (particularly F and Cl) affect a variety of processes such as the vapor saturation, depolymerizing the melt structure, and by complexing with metals, which exert strong controls on the compositional variations, style of mineralization and related mineralization processes in hydrothermal ore deposits (Loferski and Ayuso, 1995; Yardley, 2005; Zhang et al., 2012). Therefore, tracing the variation of F and Cl contents in natural melts is crucial to understanding of the factors

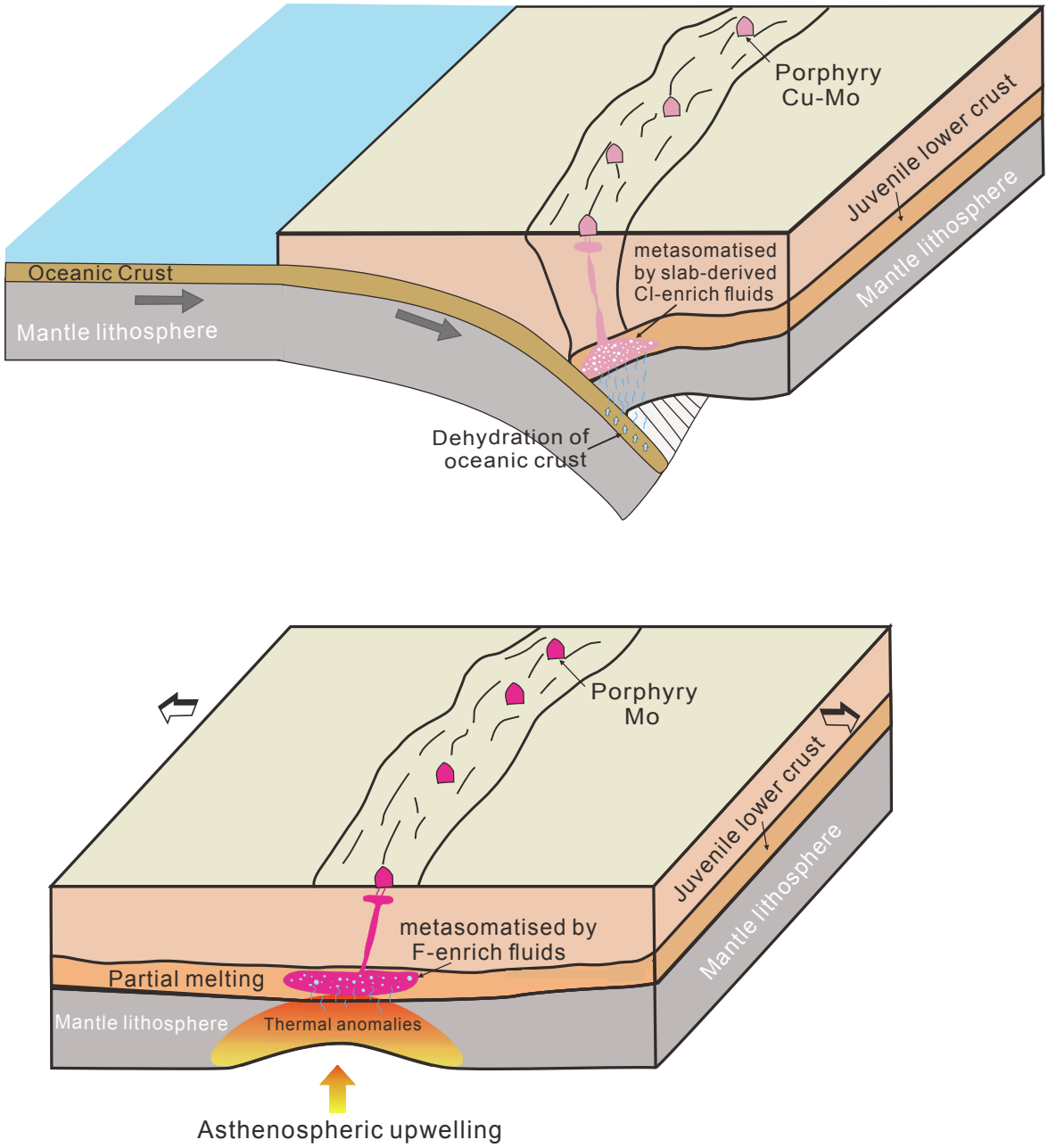


**Fig. 9.** Schematic illustration of genetic model for porphyry Cu-Mo and Mo deposits in NE China.

controlling on Cu-Mo and Mo mineralization. The apatites from the porphyry Cu-Mo mineralized granites (WS and JC) show relatively higher Cl and lower F contents than those from the porphyry Mo mineralized granites (LM, FA and DHS) (Fig. 7c). As aforementioned, these porphyry Cu-Mo and Mo deposits are located near and away from the subduction zones, respectively (Fig. 1b). As a result, the high Cl contents of the apatites from the WS and JC granites near to the subduction zone should have a source of Cl from other fluids, most likely fluids derived from a subducted slab (e.g., Kawamotoa et al., 2013; Reynard, 2013). Generally, Cl is volatile trace element that can be incorporated into some hydrous minerals (i.e., amphibole, chlorite and/or serpentine) and variously released during slab subduction (Jiang et al., 2018). The altered oceanic crust and sediments could enrich a large amount of Cl (Wang, 2015). As the subducting slab dehydration, a large amount of Cl is being contributed by the altered oceanic crust, marine sediments and mineral phase decomposes, and then preferentially enters the liquid phase (Stroncik and Haase, 2004; Liu et al., 2020). That is, near the subduction zone the juvenile crust was metasomatized by subducted slab-derived fluids with increasing Cl contents (Fig. 9), and partial melting of such a source leads to the WS and JC granites that have high Cl contents. In contrast, further away from the subduction zone under intra-continental setting, with partial melting of juvenile crust the breakdown of amphibole and/or biotite will produce a hydrous fertile magma enriched in F (Chen and Zheng, 2015; Hou et al., 2011), and making contributions to the generation of the LM, FA and DHS granites with high F contents. Besides, F is also controlled by the phengite and lawsonite, decomposing of these minerals at greater depth under higher pressure (Pagé et al., 2016; Jiang et al., 2018). Therefore, F is transported to deeper depths in the subducted oceanic crust, and released through breakdown of phengite and lawsonite, may also provide an important contribution to the formation of LM, FA and DHS granites (e.g., Jiang et al., 2018). The Cl contents of the apatites from the LM, FA and DHS granites is $<0.10\%$ but have higher F contents, similar to the apatites from porphyry Mo deposits in the Qinling area (Fig. 7c and reference in), which is consistent with their intracontinental tectonic setting characteristics. As depicted in Xing et al. (2019), apatite from the Huojihe porphyry Mo deposit adjacent to the Luming porphyry Mo deposit also have low Cl and high F contents with higher F/Cl ratios, which is compatible with the results shown in this study (Fig. 7c).

Magmatic water plays a key role in the formation of porphyry deposit (Richards, 2011a; Rohrlach and Loucks, 2005). High magmatic water contents can enhance the fertility of magmas and favor the formation of magmatic–hydrothermal ore deposits, as water is largely responsible for the dissolution, transport, and concentration of a variety of metal elements and compounds (Robb, 2005; Kelley and Elizabeth, 2009; Richards, 2011a). However, directly measuring the content of magmatic water is difficult, primarily as a result of the extensive degassing of magma as it reaches the shallow crust. Apatite is an important host for volatiles F, Cl, and OH (Mathez and Webster, 2005; McCubbin et al., 2015), though the minor proportion of OH in apatite, many studies have used the OH concentration of apatite to estimate $H_2O$ abundances in the melt from which the apatites crystallized (Boyce et al., 2010; McCubbin et al., 2012; Tartèse et al., 2013). Boyce and Hervig (2009) found that F and OH variation in apatite matched well with F and $H_2O$ change in the coexisting melt inclusion. Thus, OH component in apatite is a useful proxy to evaluate the water content in coexisting melt. Apatites from the WS and JC granites contain higher OH contents than those from other three ore-related granites (Fig. 7a), suggesting a higher water content of parent melt. Zircon is also ubiquitous accessory mineral in intermediate to felsic igneous rocks and relatively resistant to weathering or hydrothermal alteration (Hoskin and Schaltegger, 2003). They crystallize early and could record the composition of parent melt, controlled by the relevant zircon/melt partition coefficients (Claiborne et al., 2010). Lu et al. (2016) reported that zircon compositions have great potential as a pathfinder for porphyry Cu ± Mo ± Au deposits and some distinct zircon trace element ratios (e.g., (Ce/Nd)/Y, Dy/Yb ratios) can be used to indicate the magmatic water contents. That's because trace element proxies for the ratio of hornblende in the differentiation series up to the stage sampled are especially useful indicators of the hydration state of the melt (Davidson et al., 2013; Loucks, 2014). Amphibole preferentially incorporates middle REE (e.g., Dy) and Y over HREE (e.g., Yb; Davidson et al., 2007). In hydrous melts, hornblende crystallizes at an early stage in magmatic evolution should decrease the Dy/Yb ratio and depletes Y in the residual melt. Here, zircon crystals from the WS and JC granites have higher (Ce/Nd)/Y and lower Dy/Yb ratios than those from the other three ore-related rocks, also implying that the WS and JC magma had higher water contents (Supplementary Table 4 and Fig. 7b; Collins et al., 2016; Lu et al., 2016). Additionally, the lower whole rock Zr saturation temperatures from the WS and JC granites than those from the LM, FA and DHS granites (Supplementary Table 1), which may due to the parent melt of porphyry Cu-Mo system was more hydrous. Based on the above discussion, we noted that the water content of parent melt of porphyry Cu-Mo deposits in NE China is higher than those of porphyry Mo deposits. This conclusion is consistent with the Candela and Holland (1986), who reported that porphyry Mo-(Cu) deposits relative to porphyry Cu-(Mo), commonly related to magmas with somewhat lower initial water content.

### 6.3. Porphyry Cu-Mo and Mo deposits genetic model

Oceanic slab generally contains high concentrations of Cu (60–125 ppm; Sun et al., 2003) that are two to four times higher than typical Cu concentrations within the mantle (30 ppm; McDonough and Sun, 1995), meaning that the subducted oceanic slab material is likely to be the main source of Cu within the deposit in the study area (e.g., He et al., 2019). Crustal materials are significantly more enriched in Mo than the mantle suggested that the Mo within porphyry Mo deposits is derived from crustal material (Palme and O'Neill, 2003). In addition, many studies showed that Mo is associated with magmas melted from continental crustal materials (e.g., Farmer and DePaolo, 1984; Klemm et al., 2008; Richards, 2011b). Gao et al. (2017) concluded that partial melting of juvenile lower crust, rather than ancient crust or continental lithospheric mantle played an important role in the genesis of felsic magmas associated with the large-scale Mo mineralization in the Central Asian metallogenic domain.

It is widely considered that Cl-rich fluids are more favorable for extracting Cu from melt and in the form of chloride complexes in moderate salinity fluids transporting it (Keppler and Wyllie, 1991; Bai and Koster van Groos, 1999). Meanwhile, the increase in the Cl content will markedly increase Cu solubility (Keppler and Wyllie, 1991; Archibald et al., 2002). In comparison, porphyry Mo systems are F-rich (e.g., Audétat, 2015; Jin et al., 2018). F in fluids have important effects on partitioning Mo between melt and fluid and transporting Mo (Candela and Holland, 1984; Bai and Koster van Groos, 1999). The $D_{Mo}^{fluid/melt}$ was higher in the F-containing system than in the presence of Cl (Keppler and Wyllie, 1991). Indeed, the F enrichment in the LM, FA and DHS porphyry can promote high degrees of melt fractionation by lowering the magma solidus to extend the crystallization interval, and by lowering the melt viscosity to facilitate residual melt extraction and accumulation in the apical regions of magma chambers (Giordano et al., 2004; Audétat, 2015). Therefore, the enrichment of Cl and lower F/Cl ratios of the apatite from the WS and JC granites compared to those from the FA, LM and DHS granites suggest that high Cl content is critical for extracting Cu from the melt and transporting Cu for the formation of Cu–Mo deposits, whereas the magma with F-rich is beneficial to Mo mineralization.

Porphyry Mo deposits that produce Mo as a main commodity have recently been divided according to tectonic setting into subduction-, rift-, and collision-types, which are also termed Endako-, Climax-, and Dabie-types (Chen and Santosh, 2014). In contrast, previous study shows that the arc magmas derived from the partial melting of metasomatized mantle wedge overlying a subducting oceanic slab are

metalliferous and can provide significant quantities of Cu (de Hoog et al., 2004; Richards, 2015), so the Cu mineralization is closely related to these arc materials (e.g., Sillitoe, 2010; Richards, 2015). Candela and Piccoli (2005) reported that intrusions in subduction settings associated with the genesis of porphyry Cu system worldwide are consistent with partial melting of hydrated mantle followed by fractionation and interaction with crustal materials. Overall, Porphyry Cu and Mo deposits are generally thought to be associated with mature island or continental arcs, although more recent research has identified porphyry deposits that formed in syn- to post-collisional settings (Hou and Cook, 2009; Hou et al., 2020; Richards, 2011b, 2015). Given that the apatite geochemistry discussed here with previously obtained geochronological data indicate that the formation of porphyry Cu-Mo deposits in NE China is in a subduction tectonic setting while the porphyry Mo deposits is in an intra-continental environment. We propose a formation model for porphyry Cu-Mo and Mo deposits in NE China as shown in Fig. 9. Fluids released from the subducted are usually $H_2O$-rich and can therefore carry significant amounts of Cu, LILE, Cl, and S (e.g., Sillitoe, 2010; He et al., 2019). The juvenile crust was metasomatized by this fluid accompanied by the enrichment of Cu and Cl, with decreasing in solidus temperatures. Long-lived subduction causing partial melting of juvenile crust material with Cu-enriched, and eventually to form the $H_2O$-rich, and Cl-rich granites in WS and JC porphyry Cu-Mo deposits (Fig. 9). In contrast, when the tectonic setting transforms from continental arc to intra-continental environment, accompanying with upwelling of hot asthenosphere, the F-enriched fluids released by these long-term metamorphic dehydration reactions and has been stored at the juvenile lower crust. Here, the melting of the partial melting of such a source eventually leading to a Mo-enriched magma. The magma emplaced shallow crust to generate the granites and their related Mo deposits in the NE region (e.g., the LM, FA and DHS porphyry Mo deposits; Fig. 9).

## 7. Conclusions

In this study, an integrated investigation on in-situ elemental and isotopic geochemistry of apatite from the porphyry Cu-Mo and Mo deposits in NE China, to discriminate Cu-Mo and Mo mineralization. The main conclusion is as follows:

(1) The Wunugetushan, Jinchanggou, Luming, Fu'anpu and Daheihan porphyry Cu-Mo/Mo deposits are generated by partial melting of juvenile crustal material.
(2) Apatite from the porphyry Cu-Mo mineralized granites have higher Cl/F ratios, OH contents, and fluid-mobile elements Ba and Sr, suggesting that the magmatic source of porphyry Cu-Mo deposits were more hydrous and modified by subducted slab-derived Cl-enriched fluids with carry significant amounts of Cu.
(3) Apatite from the porphyry Mo mineralized granites have high F with lower Cl/F ratios, indicating that these granites formed in juvenile crustal dehydration self-metasomatism with released F-enriched fluids under the intra-continental environment.

## Declaration of Competing Interest

The authors declare that they have no known competing financial interests or personal relationships that could have appeared to influence the work reported in this paper.

## Acknowledgements

This work was supported by the National Key R&D Program of China (2016YFC0600403) and Science and Technology Planning Project of Guangdong Province, China (2020B1212060055). We thank the Dr. Xing Chang-Ming, Zhang Le, Wu Dan, Zhang Di and Ying Yuan-Can for helping with analytical works. Two reviewers and editor are also sincerely thanked for their constructive reviews and comments.This is contribution No.IS-3023 from GIGCAS.

## Appendix A. Supplementary data

Supplementary data to this article can be found online at https://doi.org/10.1016/j.oregeorev.2021.104218.

## References

Archibald, S.M., Migdisov, A.A., Williams-Jones, A.E., 2002. An experimental study of the stability of copper chloride complexes in water vapor at elevated temperatures and pressures. Geochim. Cosmochim. Acta 66 (9), 1611–1619.
Audétat, A., 2015. Compositional evolution and formation conditions of magmas and fluids related to porphyry Mo mineralization at Climax, Colorado. J. Petrol. 56, 1519–1546.
Bai, T.B., Koster van Groos, A., 1999. The distribution of Na, K, Rb, Sr, Al, Ge, Cu, W, Mo, La, and Ce between granitic melts and coexisting aqueous fluids. Geochim. Cosmochim. Acta 63, 1117–1131.
Barth, A.B., Walshe, J.L., Cloutier, J., Verrall, M., Cleverley, J.S., Pownceby, M.I., Macrae, C.M., Wilson, N.C., Tunjic, J., Nortje, G.S., Robinson, P., 2013. Biotite and apatite as tools for tracking pathways of oxidized fluids in the Archean East Repulse gold deposit, Australia. Econ. Geol. 108, 667–690.
Bizzarro, M., Simonetti, A., Stevenson, R.K., Kurszlaukis, S., 2003. In situ $^{87}Sr/^{86}Sr$ investigation of igneous apatites and carbonates using laser-ablation MC-ICP-MS. Geochim. Cosmochim. Acta 67 (2), 289–302.
Bouzari, F., Hart, C.J.R., Bissig, T., Barker, S., 2016. Hydrothermal alteration revealed by apatite luminescence and chemistry: a potential indicator mineral for exploring covered porphyry copper deposits. Econ. Geol. 111 (6), 1397–1410.
Boyce, J.W., Hervig, R.L., 2009. Apatite as a monitor of late-stage magmatic processes at Volcán Irazú, Costa Rica. Contrib. Miner. Petrol. 157, 135–145.
Boyce, J.W., Liu, Y., Rossman, G.R., Guan, Y.B., Eiler, J.M., Stolper, E.M., Taylor, L.A., 2010. Lunar apatite with terrestrial volatile abundances. Nature 466, 466–470.
Bruand, E., Storey, C., Fowler, M., 2014. Accessory mineral chemistry of high Ba–Sr granites from northern Scotland: constraints on petrogenesis and records of whole-rock signature. J. Petrol. 55, 1619–1651.
Cai, W.Y., Wang, Z.G., Li, J., Fu, K.Y., Konare, Y., Li, S.D., 2019. Zircon U-Pb and molybdenite Re–Os geochronology and geochemistry of Jinchang porphyry gold–copper deposit, NE China: two-phase mineralization and the tectonic setting. Ore Geol. Rev. 107, 735–753.
Candela, P.A., Holland, H.D., 1984. The partitioning of Cu and Mo between silicate melt and aqueous fluids. Geochim. Cosmochim. Acta 48, 373–380.
Candela, P.A., Holland, H.D., 1986. A mass transfer model for copper and molybdenum in magmatic hydrothermal systems: the origin of porphyry-type ore deposits. Econ. Geol. 81, 1–19.
Candela PA, Piccoli PM., 2005. Magmatic processes in the development of porphyry-type ore systems. Econ Geol 100th Anniversary. pp. 25–38.
Cao, M., Evans, N.J., Qin, K., Danišík, M., Li, G., McInnes, B.I.A., 2019. Open apatite Sr isotopic system in low-temperature hydrous regimes. J. Geophys. Res. Solid Earth 124, 11192–11203.
Chen, H.Y., Wu, C., 2020. Metallogenesis and major challenges of porphyry copper systems above subduction zones. Sci. China Earth Sci. 63, 899–918.
Chen, L., Yan, Z., Wang, Z.Q., Wang, K.M., 2017a. Characteristics of apatite from 160–140 Ma Cu(Mo) and Mo(W) deposits in East Qinling. Acta Geol. Sin. 91, 1925–1942 (in Chinese with English abstract).
Chen, L., Zhang, Y., 2018. In situ major-, trace-elements and Sr-Nd isotopic compositions of apatite from the Luming porphyry Mo deposit, NE China: constraints on the petrogenetic-metallogenic features. Ore Geol. Rev. 94, 93–103.
Chen, W., Simonetti, A., 2014. Evidence for the multi-stage petrogenetic history of the Oka carbonatite complex (Québec, Canada) as recorded by perovskite and apatite. Minerals 4, 437–476.
Chen, X., Wang, J.X., Zhang, Z.Z., Liu, R.F., 2010a. Major element features of ore-bearing rock in Jinchanggou copper-molybdenum deposit of Jidong, Heilongjiang and its tectonic setting. Global Geol. 29, 51–55 (in Chinese with English abstract).
Chen, Y.J., Santosh, M., 2014. Triassic tectonics and mineral systems in the Qinling Orogen, central China. Geol. J. 49, 338–358.
Chen, Y.X., Zheng, Y.F., 2015. Extreme Nb/ta fractionation in metamorphic titanite from ultrahigh-pressure metagranite. Geochim. Cosmochim. Acta 150, 53–73.
Chen, Y.J., Zhang, C., Li, N., Yang, Y.F., Deng, K., 2012. Geology of the Mo deposits in Northeast China. J. Jilin Univ. (Earth Sci. Ed.) 42, 1223–1268 (in Chinese with English abstract).
Chen, Y.J., Zhang, C., Wang, P., Pirajno, F., Li, N., 2017b. The Mo deposits of Northeast China: a powerful indicator of tectonic settings and associated evolutionary trends. Ore Geol. Rev. 81, 602–640.
Chen, Z.G., Zhang, L.C., Wan, B., Wu, H.Y., Cleven, N., 2011. Geochronology and geochemistry of the Wunugetushan porphyry Cu-Mo deposit in NE China, and their geological significance. Ore Geol. Rev. 43, 92–105.
Chen, Z.G., Zhang, L.C., Lu, B.Z., Li, Z.L., Wu, H.Y., Xiang, P., Huang, S.W., 2010b. Geochronology and geochemistry of the Taipingchuan copper-molybdenum deposit in Inner Mongolia, and its geological significances. Acta Petrol. Sinica 26, 1437–1449 (in Chinese with English abstract).
Cheng, G.H., Wang, R.L., Zeng, Q.D., Guo, Y.P., Duan, X.X., Wei, J.J., Zhang, J.S., Gao, X.H., 2015. Zircon U-Pb ages, Hf isotopes of the granitoids and Re-Os ages of the

molybdenites in Luming molybdenum ore area, Heilongjiang Province, and its geological significance. Acta Petrol. Sinica 31 (8), 2450–2464.
Chu, M., Wang, K., Griffin, W.L., Chung, S., O'Reilly, S.Y., Pearson, N.J., Iizuka, Y., 2009. Apatite composition: tracing petrogenetic processes in Transhimalayan granitoids. J. Petrol. 50, 1829–1855.
Claiborne, L.L., Miller, C.F., Wooden, J.L., 2010. Trace element composition of igneous zircon: a thermal and compositional record of the accumulation and evolution of a large silicic batholith, Spirit Mountain, Nevada. Contrib. Mineral. Petrol. 160, 511–531.
Cogné, J.P., Kravchinsky, V.A., Halim, N., Hankard, F., 2005. Late Jurassic-Early Cretaceous closure of the Mongol-Okhotsk Ocean demonstrated by new Mesozoic palaeomagnetic results from the Trans-Baïkal area (SE Siberia). Geophys. J. Int. 163, 813–832.
Collins, W.J., Huang, H.Q., Jiang, X.Y., 2016. Water-fluxed crustal melting produces Cordilleran batholiths. Geology 2, 143–146.
Cooke, D.R., 2005. Giant porphyry deposits: characteristics, distribution, and tectonic controls. Econ. Geol. 100 (5), 801–818.
Creaser, R.A., Gray, C.M., 1992. Preserved initial $^{87}Sr$ in apatite from altered felsic igneous rocks: a case study from the Middle Proterozoic of South Australia. Geochim. Cosmochim. Acta 56, 2789–2795.
Davidson, J., Turner, S., Handley, H., Macpherson, C., Dosseto, A., 2007. Amphibole "sponge" in arc crust? Geology 35, 787–790.
Davidson, J., Turner, S., Plank, T., 2013. Dy/Dy*: Variations arising from mantle sources and petrogenetic processes. J. Petrol. 54, 525–537.
de Hoog, J.C.M., Hattori, K.H., Hoblitt, R.P., 2004. Oxidized sulfur-rich mafic magma at Mount Pinatubo, Philippines. Contrib. Miner. Petrol. 146 (6), 750–761.
Deng, K., Li, Q.G., Chen, Y.J., Zhang, C., Zhu, X.F., Xu, Q.W., 2018. Geochronology, geochemistry and Sr-Nd-Pb-Hf isotopes of the Early Jurassic granodiorite from the Sankuanggou intrusion, Heilongjiang Province, Northeastern China: petrogenesis and geodynamic implications. Lithos 296–299, 113–128.
Dmitry, V.M., Valery, A.V., Alexey, Y.K., Michael, T.D.W., 2010. Late Mesozoic tectonics of Central Asia based on paleomagnetic evidence. Gondwana Res. 18, 400–419.
Doherty, A.L., Webster, J.D., Goldoff, B.A., Piccoli, P.M., 2014. Partitioning behavior of chlorine and fluorine in felsic melt-fluid(s)-apatite systems at 50 MPa and 850–950 °C. Chem. Geol. 384, 94–109.
Dokuz, A., Aydin, F., Karsh, O., 2020. Postcollisional transition from subduction- to intraplatetype magmatism in the eastern Sakarya zone, Turkey: indicators of northern Neotethyan slab breakoff. GSA Bull. 131, 1623–1642.
Douce, A.E.P., Roden, M.F., Chaumba, J., Fleisher, C., Yogodzinski, G., 2011. Compositional variability of terrestrial mantle apatites, thermodynamic modeling of apatite volatile contents, and the halogen and water budgets of planetary mantles. Chem. Geol. 288, 14–31.
Du, J.G., Wang, G.W., Jia, L.H., 2019. In situ major and trace element compositions of apatites from Luanchuan orecluster: Implications for porphyry Mo mineralization. Ore Geol. Rev. 115, 103174.
Elliott, T., Plank, T., Zindler, A., White, W., Bourdon, B., 1997. Element transport from slab to volcanic front at the Mariana arc. J. Geophys. Res. Solid Earth 102, 14991–15019.
Farmer, G.L., Depaolo, D.J., 1984. Origin of Mesozoic and Tertiary granite in the western United States and implications for Pre-Mesozoic crustal structure: 1. Nd and Sr isotopic studies of unmineralized and Cu- and Mo-mineralized granite in the Precambrian Craton. J. Geophys. Res. Solid Earth 89, 10141–10160.
Gao, J., Klemd, R., Zhu, M.T., Wang, X.S., Li, J.L., Wan, B., Xiao, W.J., Zeng, Q.D., Shen, P., Sun, J.R., Qin, K.Z., Campos, E., 2017. Large-scale porphyry-type mineralization in the Central Asian metallogenic domain: a review. J. Asian Earth Sci. 165, 7–36.
Guo, X.G., Li, J.W., Zhang, D.H., Xue, F., Xian, H.B., Wang, S.J., Jiao, T.L., 2020. Petrogenesis and tectonic setting of igneous rocks from the Dongbulage porphyry Mo deposit, Great Hinggan Range, NE China: constraints from geology, geochronology, and isotope geochemistry. Ore Geol. Rev. 120, 103326.
Giordano, D., Romano, C., Dingwell, D.B., Poe, B., Behrens, H., 2004. The combined effects of water and fluorine on the viscosity of silicic magmas. Geochim. Cosmochim. Acta 68 (24), 5159–5168.
Han, S.J., Sun, J.G., Bai, L.A., Xing, S.W., Chai, P., Zhang, Y., Yang, F., Men, L.J., Li, Y.X., 2012. Geology and ages of porphyry and medium- to high-sulphidation epithermal gold deposits of the continental margin of Northeast China. Int. Geol. Rev. 55, 287–310.
Hans Wedepohl, K., 1995. The composition of the continental crust: Geochim. Cosmochim. Acta 59 (7), 1217–1232.
He, J., Wang, B.D., Wang, L.Q., Wang, Q.Y., Yan, G.C., 2019. Geochemistry and geochronology of the Late Cretaceous Tongchanggou Mo–Cu deposit, Yidun Terrane, SE Tibet; implications for post-collisional metallogenesis. J. Asian Earth Sci. 172, 308–327.
Hoskin, P.W.O., Schaltegger, U., 2003. The composition of zircon and igneous and metamorphic petrogenes. Rev. Mineral. Geochem. 53, 27–62.
Hou, X.G., 2017. Mesozoic metallogenetic granitoids from porphyry Mo deposit in the eastern Jilin-Heilongjiang provinces: Petrogenesis and Molybdenum mineralization. Doctoral thesis, Jilin University (in Chinese).
Hou, Z.Q., Cook, N.J., 2009. Metallogenesis of the Tibetan collisional orogen: a review and introduction to the special issue. Ore Geol. Rev. 36, 2–24.
Hou, Z.Q., Yang, Z.M., Wang, R., Zheng, Y.C., 2020. Further discussion on porphyry Cu-Mo-Au deposit formation in Chinese mainland. Earth Sci. Front. 27 (2), 20–44.
Hou, Z.Q., Zhang, H.R., Pan, X.F., Yang, Z.M., 2011. Porphyry Cu (−Mo−Au) deposits related to melting of thickened mafic lower crust: examples from the eastern Tethyan metallogenic domain. Ore Geol. Rev. 39, 21–45.
Hu, X.L., Ding, Z.J., He, M.C., Yao, S.Z., Zhu, B.P., Shen, J., Chen, B., 2014. A porphyry-skarn metallogenic system in the Lesser Xing'an Range, NE China: implications from U-Pb and Re-Os geochronology and Sr-Nd-Hf isotopes of the Luming Mo and Xulaojiugou Pb-Zn deposits. J. Asian Earth Sci. 90, 88–100.
Hu, X.L., Yao, S.Z., Zeng, G.P., Liu, W.H., Zhang, Z.J., 2019. Multistage magmatism resulting in large-scale mineralizaion: a case from the Huojihe porphyry Mo deposit in NE China. Lithos 326, 397–414.
Jahn, B.M., Wu, F., Chen, B., 2000. Granitoids of the central asian orogenic belt and continental growth in the phanerozoic. Trans. R. Soc. Edinb. Earth Sci. 91, 181–193.
Jiang, X.Y., Li, H., Ding, X., Wu, K., Guo, J., Liu, J.Q., Sun, W.D., 2018. Formation of A-Type granites in the Lower Yangtze River Belt: a perspective from apatite geochemistry. Lithos 304–307, 125–134.
Jin, C., Gao, X.Y., Chen, W.T., Zhao, T.P., 2018. Magmatic-hydrothermal evolution of the Donggou porphyry Mo deposit at the southern margin of the North China Craton: evidence from chemistry of biotite. Ore Geol. Rev. 92, 84–96.
Ju, N., Zhang, S., Kou, L.L., Wang, H.P., Zhang, D., Gu, Y.C., Wu, T., 2019. Source and tectonic setting of porphyry Mo deposits in Shulan, Jilin Province, China. Minerals 9 (11), 657.
Kawamotoa, T., Yoshikawa, M., Kumagai, Y., Mirabueno, M.H.T., Okuno, M., 2013. Mantle wedge infiltrated with saline fluids from dehydration and decarbonation of subducting slab. PNAS 110, 9663–9668.
Kelley, K.A., Elizabeth, C., 2009. Water and the oxidation state of subduction zone magmas. Science 325, 605–607.
Kemp, A.I.S., Hawkesworth, C.J., Foster, G.L., Paterson, B.A., Woodhead, J.D., Hergt, J. M., Gray, C.M., Whitehouse, M.J., 2007. Magmatic and crustal differentiation history of granitic rocks from Hf–O isotopes in zircon. Science 16, 980–983.
Keppler, H., Wyllie, P.J., 1991. Partitioning of Cu, Sn, Mo, W, U and Th between melt and aqueous fluid in the systems haplogranite-$H_2O$-HCl and haplogranite-$H_2O$-HF. Contrib. Miner. Petrol. 109, 139–150.
Klemm, L.M., Pettke, T., Heinrich, C.A., 2008. Fluid and source magma evolution of the Questa porphyry Mo deposit, New Mexico, USA. Mineral. Deposita 43, 533–552.
King, P., White, A., Chappell, B., Allen, C., 1997. Characterization and origin of aluminous A-type granites from the Lachlan Fold Belt, southeastern Australia. J. Petrol. 38 (3), 371–391.
Kusebauch, C., John, T., Whitehouse, M.J., Klemme, S., Putnis, A., 2015. Distribution of halogens between fluid and apatite during fluid-mediated replacemen processes. Geochim. Cosmochim. Acta 170, 225–246.
Labanieh, S., Chauvel, C., Germa, A., Quidelleur, X., 2012. Martinique: a clear case for sediment melting and slab dehydration as a function of distance to the trench. J. Petrol. 53, 2441–2464.
La Cruz, N.L., Simon, A.C., Wolf, A.S., Reich, M., Barra, F., Gagnon, J.E., 2019. The geochemistry of apatite from the Los Colorados iron oxide–apatite deposit, Chile: implications for ore genesis. Miner. Deposita 54, 1143–1156.
Li, C.Y., 2013. The source and metallogenic mechanism of porphyry molybdenum deposits. Doctoral thesis, Guangzhou Institute of Geochemistry, Chinese Academy of Sciences (in Chinese).
Li, L.X., Song, Q.H., Wang, D.H., Wang, C.H., Qu, W.J., Wang, Z.G., Bi, S.Y., Yu, C., 2009. Re-Os isotopic dating of molybdenite from the Fu'anpu molybdenum deposit of Jilin provence and discussion on its metallogenesis. Rock Mineral Analisis 28, 283–287 (in Chinese with English abstract).
Li, X.H., Li, Z.X., Li, W.X., Liu, Y., Yuan, C., Wei, G.J., Qi, C.S., 2007. U-Pb zircon, geochemical and Sr-Nd-Hf isotopic constraints on age and origin of Jurassic I- and A-type granites from central Guangdong, SE China: a major igneous event in response to foundering of a subducted flat-slab? Lithos 96, 186–204.
Li, X.H., Sun, M., Wei, G.J., Liu, Y., Lee, C.Y., Malpas, J., 2000. Geochemical and Sm–Nd isotopic study of amphibolites in the Cathaysia Block, southeastern China: evidence for an extremely depleted mantle in the Paleoproterozoic. Precambr. Res. 102, 251–262.
Liu, L., Hu, R.Z., Zhong, H., Yang, J.H., Kang, L.F., Zhang, X.C., Fu, Y.Z., Mao, W., Tang, Y.W., 2020. Petrogenesis of multistage S-type granites from the Malay Peninsula in the Southeast Asian tin belt and their relationship to Tethyan evolution. Gondwana Res. 84, 20–37.
Liu, R.B., 2016. Geology, Geochemistry and Formation Mechanism of the Huzhagaitu Porphyry Molybdenum Deposit in Inner Mongolia, NE China. Master's degree, China University of Geosciences (Beijing) (in Chinese).
Liu, Y.S., Hu, Z.C., Zong, K.Q., Gao, C.G., Gao, S., Xu, J., Chen, H.H., 2010. Reappraisement and refinement of zircon U-Pb isotope and trace element analyses by LA-ICP-MS. Chin. Sci. Bull. 55, 1535–1546.
Loferski, P.J., Ayuso, R.A., 1995. Petrography and mineral chemistry of the composite Deboullie pluton, northern Maine, USA: implications for the genesis of Cu-Mo mineralization. Chem. Geol. 123, 89–105.
Loucks, R.R., 2014. Distinctive composition of copper-ore-forming arc magmas. Aust. J. Earth Sci. 61, 5–16.
Lu, Y.J., Loucks, R.R., Fiorentini, M., McCuaig, T.C., Evans, N.J., Yang, Z.M., Hou, Z.Q., Kirkland, C.L., Parra-Avila, L.A., Kobussen, A., 2016. Zircon Compositions as a Pathfinder for Porphyry Cu±Mo±Au Deposits. Society of Economic Geologists Special Publication, pp. 329–347.
Ludwig, K.R., 2003. User's Manual for Isoplot 3.00: A Geochronological Toolkit for Microsoft Excel. Berkeley Geochronology Center Special Publication. pp, 1–74.
Mao, M., Rukhlov, A.S., Rowins, S.M., Spence, J., Coogan, L.A., 2016. Apatite trace Element compositions: a robust new tool for mineral exploration. Econ. Geol. 111, 1187–1222.
Mathez, E.A., Webster, J.D., 2005. Partitioning behavior of chlorine and fluorine in the system apatite-silicate melt-fluid. Geochim. Cosmochim. Acta 69, 1275–1286.

McCubbin, F.M., Hauri, E.H., Elardo, S.M., Vander Kaaden, K.E., Wang, J., Shearer, C.K., 2012. Hydrous melting of the martian mantle produced both depleted and enriched shergottites. Geology 40, 683–686.
McCubbin, F.M., Kaaden, K.E.V., Tartèse, R., Boyce, J.W., Mikhail, S., Whitson, E.S., Bell, A.S., Anand, M., Franchi, I.A., Wang, J., 2015. Experimental investigation of F, Cl, and OH partitioning between apatite and Fe-rich basaltic melt at 1.0–1.2 GPa and 950–1000 °C. Am. Mineral. 100, 1790–1802.
McDonough, W.F., Sun, S.S., 1995. The composition of the Earth. Chem. Geol. 120, 223–253.
Mi, M., Li, C.Y., Sun, W.D., Li, D.F., Zhu, C.H., 2017. Yaochong Mo deposit, a low-F porphyry Mo deposit from the Qinling-Dabie orogenic belt. Ore Geol. Rev. 88, 188–200.
Middlemost, E.K., 1994. Naming materials in the magma/igneous rock system. Earth-Sci. Rev. 37, 215–224.
Miles, A.J., Graham, C.M., Hawkesworth, C.J., Gillespie, M.R., Hinton, R.W., 2013. Evidence for distinct stages of magma history recorded by the compositions of accessory apatite and zircon. Contrib. Miner. Petrol. 166 (1), 1–19.
Ouyang, H.G., Mao, J.W., Santosh, M., Zhou, J., Zhou, Z.H., Wu, Y., 2013. Geodynamic setting of Mesozoic magmatism in NE China and surrounding regions: perspectives from spatio-temporal distribution patterns of ore deposits. J. Asian Earth Sci. 78, 222–236.
Pagé, L., Hattori, K., de Hoog, J.C.M., Okay, A.I., 2016. Halogen (F, Cl, Br, I) behaviour in subducting slabs: a study of lawsonite blueschists in western Turkey. Earth Planet. Sci. Lett. 442, 133–142.
Palma, G., Barra, F., Reich, M., Valencia, V., Simon, A.C., Vervoort, J., Leisen, M., Romero, R., 2019. Halogens, trace element concentrations, and Sr-Nd isotopes in apatite from iron oxide-apatite (IOA) deposits in the Chilean iron belt: Evidence for magmatic and hydrothermal stages of mineralization. Geochim. Cosmochim. Acta 246, 515–540.
Palme, H., O'Neill, H.S.C., 2003. Cosmochemical estimates of mantle composition. In: Heinrich, D.H., Karl, K.T. (Eds.), Treatise on Geochemistry. Pergamon, Oxford, pp. 1–38.
Patiño Douce, A.E., 1999. What do experiments tell us about the relative contributions of crust and mantle to the origin of granitic magmas? Geol. Soc., London Spec. Publ. 168, 55–75.
Pearce, N., Perkins, W.A., Westgate, J., Gorton, M., Jackson, S., Neal, C., Chenery, S., 1997. A compilation of new and published major and trace element data for NIST SRM 610 and NIST SRM 612 glass reference materials. Geostand. Geoanal. Res 21 (1), 115–144.
Peccerillo, A., Taylor, S., 1976. Geochemistry of Eocene calc-alkaline volcanic rocks from the Kastamonu area, northern Turkey. Contrib. Miner. Petrol. 58, 63–81.
Pei, J.L., Sun, Z.M., Liu, J., Liu, J., Wang, X.S., Yang, Z.Y., Zhao, Y., Li, H.B., 2011. A paleomagnetic study from the Late Jurassic volcanics (155 Ma), North China: implications for the width of Mongol-Okhotsk Ocean. Tectonophysics 510, 370–380.
Piccoli, P.M., Candela, P.A., 2002. Apatite in igneous systems. In: Kohn, M.J., Rakovan, Hughes, J.M. (Eds.), Phosphates: geochemical, geobiological, and materials importance Rev. Mineral. Geochem., pp. 255–292.
Pirajno, F., Santosh, M., 2014. Rifting, intraplate magmatism, mineral systems and mantle dynamics in central Eurasia: an overview. Ore Geol. Rev. 63, 265–295.
Qu, P., Li, N.B., Niu, H.C., Yang, W.B., Shan, Q., Zhang, Z.Y., 2019. Zircon and apatite as tools to monitor the evolution of fractionated I-type granites from the central Great Xing'an Range, NE China. Lithos 348–349, 105207.
Reynard, B., 2013. Serpentine in active subduction zones. Lithos 178, 171–185.
Ren, Q., Zhang, S., Wu, H., Liang, Z., Miao, X., Zhao, H., Li, H., Yang, T., Pei, J., Davis, G. A., 2016. Further paleomagnetic results from the ~155 Ma Tiaojishan Formation, Yanshan Belt, North China, and their implications for the tectonic evolution of the Mongol-Okhotsk suture. Gondwana Res. 35, 180–191.
Richards, J.P., 2011a. High Sr/Y arc magmas and porphyry Cu ± Mo ± Au deposits: just add water. Econ. Geol. 106, 1075–1081.
Richards, J.P., 2011b. Magmatic to hydrothermal metal fluxes in convergent and collided margins. Ore Geol. Rev. 40, 1–26.
Richards, J.P., 2015. The oxidation state, and sulfur and Cu contents of arc magmas: implications for metallogeny. Lithos 233, 27–45.
Robb, L., 2005. In: Introduction to ore-forming processes. Blackwell Pub, Oxford, p. 373.
Rohrlach, B.D., Loucks, R.R., 2005. Multi-million-year cyclic ramp-up of volatiles in a lower crustal magma reservoir trapped below the Tampakan copper-gold deposit by Mio-Pliocene crustal compression in the southern Philippines. In: Porter, T.M. (Ed.), Super porphyry copper and gold deposits: A global perspective: Adelaide, South Australia. PGC Publishing, pp. 369–407.
Safonova, I.Y., Santosh, M., 2014. Accretionary complexes in the Asia-Pacific region: tracing archives of ocean plate stratigraphy and tracking mantle plumes. Gondwana Res. 25, 126–158.
Seedorff, E., Dilles, J., Proffett, J., Einaudi, M., Zurcher, L., Stavast, W., Johnson, D., Barton, M., 2005. Porphyry deposits: characteristics and origin of hypogene features. Econ. Geol. 100th Annuversary. pp. 51–298.
Sengör, A.M.C., Natal'in, B.A., 1996. Paleotectonics of Asia: fragments of synthesis. In: Yin, A., Harrison, T.M. (Eds.), The Tectonic Evolution of Asia. Cambridge University Press, Cambridge, pp. 486–640.
Shi, Y.M., Cui, B., Jia, W.L., 2007. Geological features of Luming molybdenum deposit at Tieli in the Heilongjiang Province. Geol. Pros. 43 (2), 19–22 (in Chinese with English abstract).
Shu, Q., Chang, Z., Lai, Y., Zhou, Y., Sun, Y., Yan, C., 2016. Regional metallogeny of Mo-bearing deposits in northeastern China, with new Re-Os dates of porphyry Mo deposits in the northern Xilamulun district. Econ. Geol. 111, 1783–1798.
Sillitoe, R.H., 2010. Porphyry copper systems. Econ. Geol. 105, 3–41.
Sinclair, W.D., 2007. Porphyry deposits, In Goodfellow, W.D., (ed.), Mineral deposits of Canada: A synthesis of major deposit-types, district metallogeny, the evolution of geological provinces, and exploration methods. Geological Association of Canada, Mineral Deposits Division. Special Publication, 5, pp. 223–243.
Stroncik, N.A., Haase, K.M., 2004. Chlorine in oceanic intraplate basalts: constraints on mantle sources and recycling processes. Geology 32 (11), 945–948.
Sun, H., Huang, Z., Li, W., Leng, C., Ma, D., Zhang, X., 2014. Chronology, geochemistry and Sr–Nd isotope studies of Jurassic intrusions in the Diyanqinamu porphyry Mo mine, central Inner Mongolia, China. J. Asian Earth Sci. 88, 85–97.
Sun, J.G., Zhang, Y., Xing, S.W., Zhao, K.Q., Zhang, Z.J., Bai, L.A., Ma, Y.B., Liu, Y.S., 2012. Genetic types, ore-forming age and geodynamic setting of endogenic molybdenum deposits in the eastern edge of Xing-Meng Orogenic Belt. Acta Petrol. Sin. 28, 1317–1332 (in Chinese with English abstract).
Sun, S.S., McDonough, W.F., 1989. Chemical and isotopic systematics of oceanic basalts: implications for mantle composition and processes. Geol. Soc. Lond Spec. Publ. 42, 313–345.
Sun, W.D., Bennett, V., Eggins, S., Arculus, R., Perfit, M., 2003. Rhenium systematics in submarine MORB and back-arc basin glasses: laser ablation ICP-MS results. Chem. Geol. 196, 259–281.
Tan, H.Y., Shu, G.L., Lv, J.C., Han, R.P., Zhang, S., Kou, L.L., 2012. LA-ICP-MS zircon U-Pb and molybdenite Re-Os dating for the Luming large-scale molybdenum deposit in Xiao Hinggan Mountains and its geological implication. J. Jilin Univ. (Earth Sci. Ed.) 42, 1757–1770 (in Chinese with English abstract).
Tang, P., Tang, J.X., Lin, B., Wang, L.Q., Tang, X.Q., 2019. Mineral chemistry of magmatic and hydrothermal biotites from the Bangpu porphyry Mo (Cu) deposit, Tibet. Ore Geol. Rev. 115, 103122.
Tartèse, R., Anand, M., Barnes, J.J., Starkey, N.A., Franchi, I.A., Sano, Y., 2013. The abundance, distribution, and isotopic composition of hydrogen in the Moon as revealed by basaltic lunar samples: implications for the volatile inventory of the Moon. Geochim. Cosmochim. Acta 122, 58–74.
Taylor, S.R., McLennan, S.M., 1985. In: The Continental Crust: its Composition and Evolution. Oxford Press, Blackwell, p. 312.
Tu, X.L., Zhang, H., Deng, W.F., Ling, M.X., Liang, H.Y., Liu, Y., Sun, W.D., 2011. Application of RESOlution in-situ laser ablation ICP-MS in trace element analyses. Geochimica 40, 83–98.
Wang, P., 2015. Comparative study of porphyry Mo mineralizaiton in continetal collision and magmatic arc–insights from Yaochong and Diyanqinamu porphyry Mo deposits. Doctoral thesis, Guangzhou insititute of geochenistry, Chinese Academy of Sciences (in Chinese).
Wang, Y.H., Zhao, C.B., Zhang, F.F., Liu, J.J., Wang, J.P., Peng, R.M., Liu, B., 2015. SIMS Zircon U-Pb and molybdenite Re–Os geochronology, Hf isotope, and whole-rock geochemistry of the Wunugetushan porphyry Cu–Mo deposit and granitoids in NE China and their geological significance. Gondwana Res. 28, 1228–1245.
Watson, E.B., Harrison, T.M., 1983. Zircon saturation revisited: temperature and composition effects in a variety of crustal magma types. Earth Planet. Sci. Lett. 64, 295–304.
Webster, J.D., Piccoli, P.M., 2015. Magmatic apatite: a powerful, yet deceptive, mineral. Elements 11, 177–182.
Whitney, D.L., Evans, B.W., 2010. Abbreviations for names of rock-forming minerals. Am. Mineral. 95, 185–187.
Wu, F.Y., Jahn, B.M., Wilde, S.A., Lo, C.H., Yui, T.F., Lin, Q., Ge, W.C., Sun, D.Y., 2003. Highly fractionated I-type granites in NE China (II): isotopic geochemistry and implications for crustal growth in the Phanerozoic. Lithos 67, 191–204.
Wu, F.Y., Sun, D.Y., Ge, W.C., Zhang, Y.B., Grant, M.L., Wilde, S.A., Jahn, B.M., 2011. Geochronology of the phanerozoic granitoids in northeastern China. J. Asian Earth Sci. 41, 1–30.
Wu, S., Zheng, Y.Y., Sun, X., 2016. Subduction metasomatism and collision-related metamorphic dehydration controls on the fertility of porphyry copper ore-forming high Sr/Y magma in Tibet. Ore Geol. Rev. 73, 83–103.
Xie, G.Q., Mao, J.W., Wang, R.T., Meng, D.M., Sun, J., Dai, J.Z., Ren, T., Li, J.B., Zhao, H. J., 2017. Origin of the Lengshuigou porphyry–skarn Cu deposit in the Zha-Shan district, south Qinling, central China, and implications for differences between porphyry Cu and Mo deposits. Mineral. Deposita 52 (4), 621–639.
Xing, K., Shu, Q.K., Lentz, D.R., Wang, F.Y., 2019. Zircon and apatite geochemical constraints on the formation of the Huojihe porphyry Mo deposit in the Lesser Xing'an Range, NE China. Am. Mineral. 105, 382–396.
Xu, L.L., Bi, X.W., Hu, R.Z., Qi, Y.Q., Tang, Y.Y., Wang, X.S., Zhu, J.J., 2016. Redox states and genesis of magmas associated with intra-continental porphyry Cu–Au mineralization within the Jinshajiang-Red River alkaline igneous belt, SW China. Ore Geol. Rev. 73, 330–345.
Xu, W.L., Pei, F.P., Wang, F., Meng, E., Ji, W.Q., Yang, D.B., Wang, W., 2013a. Spatial-temporal relationships of Mesozoic volcanic rocks in NE China: constraints on tectonic overprinting and transformations between multiple tectonic regimes. J. Asian Earth Sci. 74, 167–193.
Xu, W.L., Wang, F., Pei, F.P., Meng, E., Tang, J., Xu, M.J., Wang, W., 2013b. Mesozoic tectonic regimes and regional ore-forming background in NE China: constraints from spatial and temporal variations of Mesozoic volcanic rock associations. Acta Petrol. Sinica 29 (2), 339–353.
Yang, J.H., Wu, F.Y., Shao, J.A., Wilde, S.A., Xie, L.W., Liu, X.M., 2006. Constraints on the timing of uplift of the yanshan fold and thrust belt, North China. Earth Planet. Sci. Lett. 246, 336–352.
Yang, Y.C., Han, S.J., Sun, D.Y., Guo, J., Zhang, S.J., 2012. Geological and geochemical features and geochronology of porphyry molybdenum deposits in the Lesser Xing'an Range-Zhangguangcai Range metallogenic belt. Acta Petrol. Sin. 28, 379–390 (in Chinese with English abstract).

Yang, Y.H., Wu, F.Y., Yang, J.H., Chew, D.M., Xie, L.W., Chu, Z.Y., Zhang, Y.B., Huang, C., 2014. Sr and Nd isotopic compositions of apatite reference materials used in U-Th–Pb geochronology. Chem. Geol. 385, 35–55.
Yardley, B., 2005. Metal concentrations in crustal fluids and their relationship to ore formation. Econ. Geol. 100, 613–632.
Yu, Y., Xu, W.L., Pei, F.P., Yang, D.B., Zhao, Q.G., 2009. Chronology and geochemistry of Mesozoic volcanic rocks in the Linjiang area, Jilin Province and their tectonic implications. Acta Geol. Sin. 83 (2), 245–257.
Zajacz, Z., Halter, W.E., Pettke, T., Guillong, M., 2008. Determination of fluid/melt partition coefficients by LA-ICPMS analysis of co-existing fluid and silicate melt inclusions: Controls on element partitioning. Geochim. Cosmochim. Acta 72, 2169–2197.
Zeng, L.J., Niu, H.C., Bao, Z.W., Yang, W.B., 2017. Chemical lattice expansion of natural zircon during the magmatic-hydrothermal evolution of A-type granite. Am. Mineral. 102, 655–665.
Zeng, Q.D., Liu, J.M., Qin, K.Z., Fan, H.R., Chu, S.X., Wang, Y.B., Zhou, L.L., 2013. Types, characteristics, and time-space distribution of molybdenum deposits in China. Int. Geol. Rev. 55, 1311–1358.
Zhang, C., Holtz, F., Ma, C.Q., Wolff, P.E., Li, X.Y., 2012. Tracing the evolution and distribution of F and Cl in plutonic systems from volatile-bearing minerals: a case study from the Liujiawa pluton (Dabie orogen, China). Contrib. Miner. Petrol. 164, 859–879.
Zhang, L., Ren, Z., Nichols, A., Zhang, Y., Zhang, Y., Qian, S., Liu, J., 2014. Lead isotope analysis of melt inclusions by LA-MC-ICP-MS. J. Anal. At. Spectrom. 29, 1393–1405.
Zhang, L., Ren, Z., Xia, X., Li, J., Zhang, Z., 2015. IsotopeMaker: a Matlab program for isotopic data reduction. Int. J. Mass Spectrom. 392, 118–124.
Zhang, Y., 2013. Research on characteristics of geology, geochemistry and metallogenic mechanism of the Jurassic molybdenum deposits in the mid-east area of Jilin. Jilin University, Changchun (in Chinese with English abstracrt).
Zheng, W., Yu, X.F., 2017. Geochronological and geochemical constraints on the petrogenesis and geodynamic setting of the Daheishan porphyry Mo deposit, Northeast China. Resour. Geol. 68 (1), 1–21.
Zheng, Y.F., Xia, Q.X., Chen, R.X., Gao, X.Y., 2011. Partial melting, fluid supercriticality and element mobility in ultrahigh-pressure metamorphic rocks during continental collision. Earth Sci. Rev. 107, 342–374.
Zhou, L.L., Zeng, Q.D., Liu, J.M., Friis, H., Zhang, Z.L., Duan, X.X., Chu, S.X., 2015. Ore genesis and fluid evolution of the Daheishan giant porphyry molybdenum deposit, NE China. J. Asian Earth Sci. 97, 486–505.
Zhou, L.L., Zeng, Q.D., Liu, J.M., Friis, H., Zhang, Z.L., Duan, X.X., Lan, T.G., 2014. Geochronology of magmatism and mineralization of the Daheishan giant porphyry molybdenum deposit, Jilin Province, Northeast China: constraints on ore genesis and implications for geodynamic setting. Int. Geol. Rev. 56 (8), 929–953.
Zhou, Y.T., Lai, Y., Meng, S., Shu, Q.H., 2018. Controls on different mineralization styles of the Dongbulage Mo and Taibudai Cu-(Mo) porphyry deposits in the Great Xing'an Range, NE China. J. Asian Earth Sci. 165, 79–95.